# Accepted Manuscript

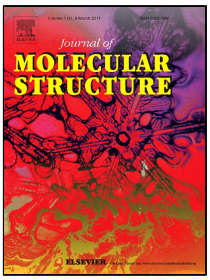


Spectral Characterization, Thermal and Biological Activity Studies of Schiff Base Complexes Derived from 4,4′-Methylenedianiline, Ethanol Amine and Benzil

Sanaa Moustafa Emam

| | |
|---|---|
| PII: | S0022-2860(16)31390-4 |
| DOI: | 10.1016/j.molstruc.2016.12.071 |
| Reference: | MOLSTR 23269 |
| To appear in: | *Journal of Molecular Structure* |
| Received Date: | 24 June 2016 |
| Revised Date: | 22 December 2016 |
| Accepted Date: | 24 December 2016 |

Please cite this article as: Sanaa Moustafa Emam, Spectral Characterization, Thermal and Biological Activity Studies of Schiff Base Complexes Derived from 4,4′-Methylenedianiline, Ethanol Amine and Benzil, *Journal of Molecular Structure* (2016), doi: 10.1016/j.molstruc.2016.12.071

**Highlights**

- Preparation of new metal complexes using in situ reaction.
- Comparing the IR spectra of metal oxides resulted from thermal decomposition of metal complexes with that of their metal complexes.
- XRD spectra of metal complexes and their final product were also carried out to calculate their crystallite size.
- Biological activity of metal complexes against Land Snails and Hepatocellular Carcinoma cell (Hep-G2).

# *Spectral Characterization, Thermal and Biological Activity Studies of Schiff Base Complexes Derived from 4,4'-Methylenedianiline, Ethanol Amine and Benzil*

**Sanaa Moustafa Emam***

*Chemistry Department, Faculty of Science, Menoufia University, Shebin El-Kom, Egypt*

**Abstract**

Some new metal(II) complexes of asymmetric Schiff base ligand were prepared by template technique. The shaped complexes are in binuclear structures and were explained through elemental analysis, molar conductivity, various spectroscopic methods (IR, U.V-Vis, XRD, ESR), thermal (TG) and magnetic moment measurements. The IR spectra were done demonstrating that the Schiff base ligand acts as neutral tetradentate moiety in all metal complexes. The electronic absorption spectra represented octahedral geometry for all complexes, while, the ESR spectra for Cu(II) complex showed axially symmetric g-tensor parameter with $g_{//} > g_{\perp} > 2.0023$ indicating to $^{2}B_{1g}$ ground state with $(d_{x2-y2})^{1}$ configuration. The nature of the solid residue created from TG estimations was affirmed utilizing IR and XRD spectra. The biological activity of the prepared complexes was studied against Land Snails. Additionally, the in vitro antitumor activity of the synthesized complexes with Hepatocellular Carcinoma cell (Hep-G2) was examined. It was observed that Zn(II) complex (**5**), exhibits a high inhibition of growth of the cell line with $IC_{50}$ of 7.09 *µg/ml*.

*Key words*: Metal complexes; IR spectra; Thermogravimeteric analysis; powder X-ray diffraction; Biological activity

## 1. Introduction

Metal coordination compounds have wide assorted qualities of technological and modern applications ranging from catalysis to anti-tumor drugs. Schiff base complexes have numerous applications in modern and biological systems [1-10]. Chelate metal complexes having high-luminance blue transmitting nature find use as materials for RGB (red, green, and blue) emission. The complexes containing oxygen and nitrogen

*Corresponding author mail: sanaa.mostafa74@yahoo.com

atoms go about as models for metalloproteins, metalloenzymes which catalyze the reduction of nitrogen and oxygen [11]. Likewise, this kind of complexes assumed an important role in life; they demonstrated high catalytic activity, antiviral, threatening to tumor, and anti-inflammatory agents [12].

Multifunctional ligands represent one of the most important compounds because of their applications in catalysis, supramolecular chemistry, medicinal inorganic chemistry research, numerous new and exciting difficulties lie ahead [13]. Metal complexes of multifunctional ligands assume an imperative part in muting the potential toxicity of a metallodrug to have a positive impact in fields of diagnosis and therapy [14].

4,4`-Methylenedianiline (MDA) is utilized as intermediate in synthesis of polyurethane froths, thermoplastics, preparation of azodyes [15] and used as antioxidant agent for lubricating oils, elastic preparing and curing specialists for epoxy resins, urethane elastomers, a corrosion safeguard for iron. MDA has possibly unsafe consequences for animals and human wellbeing. While, in people, oral or dermal exposure or inhalation of MDA has prompted inconveniences in liver digestion system with altogether expanded action of liver proteins [16]. The high flexibility of MDA is a decent candidate in the effort to prepare flexible multifunctional Schiff bases by coordination with an assortment of aldehydes and ketones. This kind of ligands can react with metal ions giving complexes with suitable properties for practical and biological applications [17]. The most well-known rout for preparation of the multifunctional Schiff base ligands is the condensation of primary diamines with dicarbonyl compounds. A carful literature study demonstrated that the metal complexes of multifunctional Schiff bases containing MDA, benzil and ethanolamine were not beforehand reported so, this kind of ligands must be prepared in two stages. The first is the synthesis of (bis-((E)- 2-(4-ethylphenylimino)-1,2-diphenylethanone) obtained from the reaction of MDA with benzil with (1:2) molar ratio in ethanol. The got ligand contains two free carbonyl groups accessible for the condensation with ethanolamine with (1:2) molar

ratio in the second step. While, in this stage numerous endeavors have been done to separate this ligand, yet all endeavors were unsuccessful even under various conditions. Henceforth, template reactions have been broadly used for the preparation of Mn(II), Co(II), Ni(II), Cu(II) and Zn(II) complexes of Schiff base ligand isolated from MDA, benzil and ethanolamine in which the metal ions are largely utilized as template agent [18,19]. These complexes were described by a few physicochemical methods as IR, $^{1}$H NMR, ESR, electronic spectra, elemental analysis, thermal studies, X-ray diffraction, magnetic susceptibilities and conductance estimations. Besides, the biological screening of metal(II) complexes against Land Snails and Hepatocellular Carcinoma cell (Hep-G2) was assessed.

## 2. Experimental

### 2.1. Analytical and Physical Measurements

All chemicals were of analytical grade (BDH, Sigma or Aldrich) and were utilized as got without further purification.

Elemental analyses (C, H, and N) have been performed on a Perkin Elmer-2400 elemental analyzer at Main Defense Chemical Laboratory. Manganese(II), cobalt(II), nickel(II) and copper(II) ions of metal complexes were estimated by complexometric titration, while, zinc(II) ion was determined by means of gravimetric analyses [20]. Additionally, the chloride ions were evaluated by utilizing Mohr's technique [20].

The infrared spectra were recorded as KBr plates on a Nicolet FT-IR spectrophotometer in the reach 4000-400cm$^{-1}$. Molar conductivity estimations were made in DMSO solution ($10^{-3}$ M) using a type CD6N Tacussel conductimeter. Magnetic susceptibilities were measured at room temperature by an modified Gouy method by utilizing a Johnson Matthey magnetic susceptibility balance. Diamagnetic corrections were determined using Pascal's constants [21]. The effective magnetic moments were ascertained from the mathematical statement $\mu_{eff} = 2.84(X_M^{corrt}\,T)^{1/2}$ where, $X_M^{corrt}$ is the molar magnetic susceptibility corrected for diamagnetism of all atoms in the compounds. The $^{1}$H NMR spectra were done in DMSO-$d_6$ on a Varian Gemini 200 NMR spectrophotometer at 300

MHz. The electron spin resonance (ESR) spectrum for Cu(II) complex was performed utilizing a Varian E-109C model spectrometer outfitted with a field modulation unit at frequency 100 kHz. Estimations were affected in the X-band on a microcrystalline powder at room temperature; the microwave force was around 10 mW. The absorption electronic spectra were measured in Nujol mulls on a Perkin Elmer Lambda 4B spectrophotometer. The thermal analysis (TG) was done by using a Shimadzu DAT/TG-50 thermal analyzer with a heating rate of 10°C/min under $N_2$ environment with a streaming rate of 20 mL/min from the room temperature up to 900°C utilizing platinum crucibles. Powder X-ray diffraction designs for complexes (**1-5**) and their final products acquired from TG examination were measured utilizing X-ray diffractometer equipped with a graphite monochromator in the range (2θ=4-80◦) by nickel separated $CuK_\alpha$ radiation (λ= 1.5418 A◦). The average crystallite size of complexes (**1-5**) and their final products obtained from TG analysis was estimated using Debeys-Scherrer equation [22]. Melting points were measured by using Stuart melting point apparatus. Biochemical measurements were carried out at Plant Protection Researches Institute, Giza, Egypt and the Regional Center for Mycology and Biotechnology, Egypt.

***2.2. Cytotoxicity assay***

Anticancer activity was carried out in Regional Center for Mycology and Biotechnology, Al-Azhar University, Cairo, Egypt. The metal complexes **(1-5),** MDA, benzil were screened for their cytotoxicity in *vitro*, in comparison with doxorubicin (DOX) as a reference drug against human-hepatic carcinoma cell line, Hep-G2. The tumor cell lines were kept up in Dulbecco's modified Eagle's medium (DMEM) supplemented with 10% heat inactivated fetal calf serum (GIBCO). Cells ($10^4$ cells/ well) were incubated at 37°C for 48 h in humidified atmosphere containing 5% $CO_2$ before treatment with the tested compounds to allow attachment of cell to the wall of the plate. Six concentrations (1.56, 3.125, 6.25, 12.50, 25.0 and 50.0 *μg/mL*) of complexes (**1-5**) were prepared by using DMSO as a diluent, at that point, 0.2 mL of each concentration of test compounds and the standard drug (doxorubicin) was added to every

cell line and incubated at 37 °C for 24 h, in a humidified 5% $CO_2$ atmosphere. Cells survival was estimated at the end of the incubation period. Viable cells yield was determined by colorimetric method [23]. The viable cell number is inversely proportional to the concentration of each complex. The compound concentrations which give 50% growth inhibition are referred to as the $IC_{50}$ and values were obtained mathematically from the concentration response curve using a computer program for probity analysis.

### *2.3. Biological Activity*

Two sorts of land snail were gathered from untreated fields and decorative plants at Menoufia governorate, Egypt; they are the glassy clover snail, *Monacha obstructa* and the brown garden snail, *Eobania vermiculata*. Muslin sacks were utilized to transfer the snails straightforwardly to the laboratory. At that point, they are kept for two weeks in little plastic boxes that contain 8-10 cm moist optimal soil supplied with fresh green lettuce leaves. At first, healthy adult snails with the same shell width were chosen for every treatment and incubated for 24 h. Based on the thin layer film system [24], five concentrations of the tested compounds were readied utilizing refined water and DMSO, then 2 mL of every concentration were stored and dispersed on the base of a petri dish by moving the dish delicately in circles. Under room conditions, solvents were evaporated leaving a thin layer of the applied concentration of the tested compounds. Five snails of the tried species were taken and exposed to the candidate concentration of the tested compounds for 72 h, then exchanged to another plastic box (24× 10 ×12 cm), shut with muslin material containing ideal soil (3-5 cm). The last experiment must be repeated with a parallel control test utilizing water and DMSO. Dead snails were numbered and expelled from the containers each 24 h. Probity analysis was used to compute $LC_{50}$ values [25].

### *2.4. Synthesis of Schiff base metal complexes obtained by template reaction of MDA, benzil and ethanolamine*

A few endeavors to synthesize the free Schiff base ligand were unsuccessful. Subsequently, all the complexes were synthesized by template reaction with molar ratio (1MDA: 2Benzil: 2Ethanol amine: 2M). 0.02 mol of a hot ethanolic solution of benzil was added to 0.01 mol of MDA in 25 mL ethanol. The reaction mixture was refluxed for 2 h at 50°C, then, 0.02 mol of ethanolamine was added to the mixture followed by reflux for 60 minutes. 0.02 mol of proper metal(II) chloride in 20 mL ethanol was added dropwise to the reactants and few drops of concentrated $H_2SO_4$ were added to the reaction mixture. It was refluxed for 3 h at 70°C. The formed complex was filtered off, washed a few times with ethanol and dried in a vacuum desiccator anhydrous $CaCl_2$ and $P_2O_5$.

## 3. Results and Discussion

### *3.1. Chemistry*

A few trials to synthesize the free Schiff base ligand derived from the condensation of 4,4'-methylenedianiline, ethanolamine with benzil, were unsuccessful. But, the metal complexes were prepared by tempelate reaction using the chloride salts of Mn(II), Co(II), Ni(II), Cu(II) and Zn(II) ions with molar ratio (1MDA: 2Benzil: 2Ethanol amine: 2M) affording metal complexes (**1-5**). The suggested structures for the prepared complexes were presented in Scheme (1). The structure of these complexes was identified using analytical and spectral methods.

**Insert Scheme (1) and its caption here**

### *3.2. Analytical data*

Table (1) demonstrates the colors, elemental analyses, stoichiometry, melting points and molar conductivity of the metal complexes separated by template reaction. We report that few endeavors to incorporate the hexadentate Schiff base ligand from the direct reaction of 4,4′-methylenedianiline, benzile and ethanolamine, failed, resulting instead in tetradentate Schiff base through the metal template reaction. The analytical

data of metal complexes are given in Table (1) which show that template reactions of (MDA: benzil: ethanolamine: metal) (1:2:2:2) molar ratio might be represented by the chemical formula:

- $[M_2(L)Cl_4(H_2O)_2].nH_2O.mEtOH$, where M=Mn(II), Co(II), Ni(II), Zn(II); n=(7.5, 8.5, 5, 7) and m= (0.5, 0, 0, 0) for complexes, (**1**), (**2**), (**3**) and (**5**), respectively.
- $[Cu_2(L)Cl_3(H_2O)_3].Cl.11H_2O$, complex (**4**).

The complexes are steady, non-hygroscopic and partially dissolvable in most organic solvents, for example, methanol, ethanol, acetonitrile, DMF and freely soluble in DMSO. The molar conductivity estimations of ($10^{-3}$ M) DMSO solutions of metal complexes revealed that all complexes (except **4**) are non-electrolytes, demonstrating that the chloride ions are directly bonded to the metal ions [15,26-30]. The molar conductance value (54 $ohm^{-1}cm^2mol^{-1}$) for complex (**4**) typified (1:1) electrolytes [26-30].

***Insert Table 1 and its caption here***

### *3.3. Infrared Spectra*

The fundamental infrared spectral bands of the metal complexes are listed and shown in Table (2) and Figs (1a, 2a, 3a, 4a). The spectra of all metal complexes were compared to the spectra of parent reactants. The IR spectra confirm the presence of MDA in the complexes with the existence of absorption bands at 3027-3080; 2929-2943, 2840-2864; 1438-1444, 1226-1271 and 1147-1170 $cm^{-1}$ ascribed to aromatic, aliphatic stretching vibrations of (CH) group; asymmetric, symmetric stretching vibrations, scissoring, wagging and twisting bending vibrations of ($CH_2$) group, respectively [31]. The spectra of all metal complexes lack absorptions bands at 1600-1700 $cm^{-1}$ which could be ascribed to ν(C=O) of benzil [11,16,50], but show another absorption band at 1566-1586 $cm^{-1}$ range, may be assigned to ν(C=N) of azomethine group [31-33]. This is indicative of the involvement of benzil carbonyl groups in condensation with MDA. Furthermore, the appearance of medium bands in the spectra of all metal complexes situated at 3274-3337 and 3232-3273 $cm^{-1}$ range, attributed to

$\upsilon_{as}$ and $\upsilon_s$ of coordinated $NH_2$ group [34,35]. In addition, the existence of $NH_2$ group in structure of complexes is supported by the presence of extra absorption bands at (1610-1625) and (1100-1180 $cm^{-1}$), due to $\delta(NH_2)$ of MDA [28] and that of EA $\nu$(-C-$NH_2$), respectively [36]. Another evidence to the coexistence of $NH_2$ group is the overtone band at *ca*.(505-551 $cm^{-1}$) [31] which undergoes blue/red shift frequency upon chelation (517-538 $cm^{-1}$) suggesting $\nu$(M-N) of $NH_2$ group. Likewise, the spectra showed bands at (466-499 $cm^{-1}$), due to $\nu$(M-N) of azomethine group [37,38]. On the otherhand, the frequency band $\nu$(-$CH_2$-OH) of ethanolamine (EA) which is observed at 1080 $cm^{-1}$ exhibits low/high shift frequency upon chelation and appeared in extent 1067-1096 $cm^{-1}$ [31,32,37,39]. Also, the spectra of complexes displayed peaks at at (1100-1156 $cm^{-1}$) and (1301-1327 $cm^{-1}$) range, attributed to $\nu$(M-OH), and $\delta$(OH) of EA [36], respectively. A broad intense absorption band in the region (3388-3427 $cm^{-1}$) present in all metal complexes is probably ascribed to the presence of coordinated OH group of EA together with lattice and/or coordinated water molecules. The coordination of water with the metal ion is supported by appearance of weak to medium band at *ca* (655-682 $cm^{-1}$) due to wagging mode [40].

The results mentioned above and the stoichiometry together with IR spectral data of isolated binuclear complexes reveal that the formed Schiff base ligand acts as tetradentate moiety where it is coordinated to the metal ion *via* two imine nitrogens, one $NH_2$ nitrogen (MDA) and one OH oxygen atom of EA as shown in Scheme (1). This is indicative of the involvement of only one mole of benzil in condensation with only one $NH_2$ group of MDA and $NH_2$ group of EA leading to the formation of monoanil asymmetric Schiff base, while, the other mole of ethanol amine used as adduct in metal complexes and the other mole of benzil is hydrolysed. This was supported also by elemental analyses and thermal studies.

***Insert Table 2 and its caption here***

***Insert Figurees (1-4) and their captions here***

### *3.3. $^1$H NMR*

The $^1$H NMR spectrum of complex (**5**) in DMSO displays multiple signals at δ (6.81-6.33ppm) range assignable to protons of aromatic rings [38,41]. The spectra of complexes (**5**) show multiple bands at (4.32, 3.55, 3.40, 3.31 and 3.20 ppm), attributed to O<u>H</u>, C<u>H$_2$</u>-phenyl, C<u>H$_2$</u>-OH, N<u>H$_2$</u> and C<u>H$_2$</u>-NH$_2$ protons [41], respectively. Also, the spectrum depicts singlet signal at δ 4.78ppm, due to N<u>H$_2$</u>-phenyl [31,32,42].

### *3.4. Molecular modeling study of Mn(II) complex*

Molecular modeling studies using ($MM^+$) calculations [43,44] are performed to determine a better understanding of the geometry of the investigated compound. The molecular mechanisms (MM+) has wide applications in the field of coordination chemistry [44]. The molecular modeling of Mn(II) complex, Table (3) and Figure (5) demonstrated some of the important bond lengths and numbering of the complex Skelton. It was watched that the stability order diminishes in this way:

N(18)ethanol=C(17)benzil ≈ C(4)ring–N(14) > C(16)–C(17) ≈ C(17)–C(42) ≈ C(16)–C(36) > N(18)ethanol-C(22)ethanol > Mn(21)–O(24)ethanol≈ Mn(28)–O(30)ethanol > Mn(21)–N(18) ethanol ≈ Mn(21)–N(14)MDA > Mn(21)–Cl(26) ≈ Mn(21)–Cl(25)

***Insert Table 3 and its caption here***

***Insert Figure 5 and its caption here***

### *3.5. Electronic Spectra and Magnetic Moments*

Electronic spectral data and magnetic moment measurements provide sufficient data to establish the geometry of metal complexes. The magnetic moment values per metal ion at room temperature and the Nujol mulls electronic absorptions are given in Table (4). The spectra of the complexes show bands at (252-296), (319-324) and (438-516 nm) ranges, ascribed to π-π* electronic transitions of benzenoide system and (C=N) group; n-π* transition due to localized lone pair of electrons on nitrogen atom of azomethine group and ligand to metal charge transfer (LMCT) [45-47].

The electronic spectrum of Mn(II) complex $[Mn_2(L)Cl_4(H_2O)_2].7.5H_2O.0.5EtOH$ (**1**) displays bands near 662, 584 and 524 nm, assignable to $^6A_{1g} \rightarrow {}^4T_{1g}$ ($G^4$) ($\upsilon_1$), $^6A_{1g} \rightarrow$

$^4E_g$ ($G^4$) ($\upsilon_2$) and $^6A_{1g} \rightarrow {}^4E_g$ ($D^4$) ($\upsilon_3$) transitions, respectively. These bands suggest an octahedral geometry around Mn(II) ion [48,49].

The electronic spectrum of Co(II) complex $[Co_2(L)Cl_4(H_2O)_2].8.5H_2O$ (**2**) exhibits bands at 657 and 580 nm, corresponding to $^4T_{1g}(F) \rightarrow {}^4A_{2g}(P)$ ($\upsilon_2$) and $^4T_{1g}(F) \rightarrow {}^4T_{2g}(P)$ ($\upsilon_3$), respectively. These transitions are consistent with an octahedral Co(II) complex [50,51]. While, the electronic spectrum of Ni(II) complex $[Ni_2(L)Cl_4(H_2O)_2].5H_2O$ (**3**) shows bands at 725, 620 and 526 nm, assigned to $^3A_{2g}(F) \rightarrow {}^3T_{2g}(F)$ ($\upsilon_1$),$^3A_{2g}(F) \rightarrow {}^3T_{1g}(F)$ ($\upsilon_2$) and $^3A_{2g}(F) \rightarrow {}^3T_{1g}(P)$ ($\upsilon_3$), respectively. These bands suggest an octahedral geometry for Ni(II) complex [41,48-50,52]. Moreover, the electronic spectrum of Cu(II) complex $[Cu_2(L)Cl_3(H_2O)_3].Cl.11H_2O$ (**4**) displays bands at 662 and 541 nm, corresponding to $^2B_{1g} \rightarrow {}^2B_{2g}$ ($\upsilon_2$) and $^2B_{1g} \rightarrow {}^2E_g$ ($\upsilon_3$) transitions, respectively indicating distorted octahedral geometry for Cu(II) complex [45,47,50]. Table (4) showed that the experimental values of magnetic moment are not high as $\mu_{(S+L)}$, this is may be due to the effect of electric field of other atoms, where the molecules surrounding the metal ion restrict the orbital motion of electrons and the orbital contribution to the magnetic moment is partially quenched. The magnetic moment values for complexes (**1**,**2, 3, 4)** are 1.61, 4.06, 3.11 and 1.59 B.M., respectively, and convenient with electronic transitions to propose the octahedral geometry for those complexes [53-55]. Furthermore, the slightly low values of magnetic moment of complexes (**1-4**) may be attributed to anti-ferromagnetic interactions [56,57]. The spectra of Zn(II) complex (**5**) do not show any d-d transitions, as well as, it is a diamagnetic complex.

The proposed chemical structures for the synthesized metal complexes (based on elemental analyses and spectral methods), are represented in Scheme 1.

***Insert Table 4 and its caption here***

### *3.6. Thermal Studies*

Thermal analysis is a very useful technique in order to assess the thermal stability of materials, confirm molecular structures and identify the different types of solvent of crystallization. Figure (6) represents TG/DTG curves of complexes **(1-5)**. The observed

and the calculated data with DTG peaks are summarized in Table 5. The DTG curves of the metal complexes can be used to be analyzed using the rate equation [58-60]:

$$d\alpha/dt=K(1-\alpha)^n$$

In the last equation, (α) and (n) pointed to the decomposed fraction and the reaction order, respectively while, *K* represents the rate constant which is given by Arrhenius equation: $K=Ae^{-E^*/RT}$, where $E^*$, A, R and *T* are the activation energy, frequency factor, the gas constant and the temperature in kelvin. The initial rate method, in which $lnI$ (*I* is the intensity of the DTG or DTA curve) is plotted versus (1000/T) can be applied to calculate the activation energy ($\Delta E^*$) [58-60]. This should give a straight line, its slope is (-E*/R). The intensity (*I*) represents ($d\alpha/dt$) in DTG curve and ΔT in DTA curve [59,60] Also, the kinetic parameters ($\Delta H$, $\Delta S^*$ and $\Delta G$) were calculated using these relations:

$\Delta H= \Delta E^*-R\Delta T$; $\Delta S^*=RTln(Ah/KT)$; $\Delta G=\Delta H-T\Delta S^*$, where *K, h, R, A and T* are Boltzmann's, Planck's and gas constants, frequency factor and absolute temperature, respectively. So, the thermodynamic and kinetic parameters of the metal complexes are given in Table 6.

The thermogravimeteric curves indicate that the complexes loss their solvent of crystallization in one step (complexes **1**, **3**) or more steps (complexes **2**, **4**, **5**). The desolvation step is extended over 26-398°C temperature range. Sometimes, this process interacts with the ligand pyrolysis (complex **2**), or with the dehalogenation process/removal of coordinated water as observed in complexes (**5**) and (**4**), respectively, Table (5). After that, the desolvation stage is followed by a number of decomposition peaks in the temperature range 398-900°C producing metal oxides [41] as final residue. The nature of the solid products was established on the basis of the TG curves and confirmed by IR and XRD spectroscopy.

The correlations between the different decomposition steps of the compounds corresponding to the weight losses are discussed in terms of the proposed formula of the complexes.

***Insert Figure (6) and its caption here***

The TG curves of metal complexes exhibit mass losses in three steps for $[Mn_2(L)Cl_4(H_2O)_2].7.5H_2O.0.5EtOH$ **(1)**, $[Co_2(L)Cl_4(H_2O)_2].8.5H_2O$ **(2)**, $[Ni_2(L)Cl_4(H_2O)_2].5H_2O$ **(3)**, $[Zn_2(L)Cl_4(H_2O)_2].7H_2O$ **(5)** and five steps for $[Cu_2(L)Cl_3(H_2O)_3].Cl.\ 11H_2O$ **(4)** between 25 and 900°C.

The thermal behavior of Mn(II) complex $[Mn_2(L)Cl_4(H_2O)_2].7.5H_2O.0.5EtOH$ **(1)** and Co(II) complex $[Co_2(L)Cl_4(H_2O)_2].8.5H_2O$ **(2)** is almost similar. The thermal decomposition of complexes **(1,2)** proceeds with three main degradation stages within the temperature range (26-900°C) and (27-900°C) for complexes (**1**) and (**2**). The first one occurs within the temperature range (26-391°C) and (27-361°C); and corresponded to the removal of solvent of crystallization (0.5 EtOH+$7.5H_2O$) and ($5H_2O$) with an estimated weight losses 16.81and 9.66% for complexes (**1**) and (**2**), respectively. This step is associated with weak DTG peaks at ($T_{max.}$= 43,349 °C) and (51, 345°C) and follows a first order and kinetic activation energy values (58.02, 252.88 $KJmol^{-1}$) for complex **(1)** and (44.54, 94.81 $KJmol^{-1}$) for complex **(2)**. Considering the IR spectra of complex **(1)**, Fig. (1a,b) represents the IR spectra of complex **(1)** before and after heating up to 391°C, they are quite similar, but some changes observed in intensity and the shape of some peaks accompanied with the disappearance of bands characteristic for EtOH and hydrated water, this confirms the removal of solvent of crystallization. Furthermore, the X-ray patterns of both solvated and desolvated forms of complex (**1**) (Fig. 7a,b) are similar but the crystalinity increases after heating due to the higher number of reflections. After desolvation, the second stage appears at (391-538°C) and (361-582°C) assigned to the ligand pyrolysis, along with dehalogenation and elimination of the rest outersphere water molecules, with estimated weight losses of 48.68 and 59.27%. This step is accompanied by weak to strong DTG peaks at ($T_{max.}$= 484 °C and 449°C) and follows a first order and kinetic activation energy values (367.57 and 264.24 $KJmol^{-1}$) for Mn(II) and Co(II) complexes, respectively. The modeling structure of the Mn(II) complex (Fig, 5 and Table 3) shows that the Mn–Cl and Mn–N bonds are more

lengthen than the other bonds, this is an evidence for the proposed mechanism for the thermal decomposition pathway for complex (**1**) (Scheme 2). The second decomposition stage for complex **(1)** led to isolation of intermediate ($C_{6.5}H_{12}NO_4Mn_2Cl$) which is stable over a large temperature range (538-706°C) as shown in Fig. 6. Its structure was confirmed by IR spectra (Fig. 8a), elemental analysis and energy dispersive X-ray spectroscopy (EDX) spectra, Fig. 9.The IR spectrum, (Fig. 8b) showed the lack of absorption bands characteristic to monosubstituted, paradisubstituted phenyl rings but new peaks appeared at 3482, 2925, 1629, 1445, 1125, 1000, 877, 610 and 520 $cm^{-1}$. These bands may be attributed to coordinated OH (hydroxyl group); υ(C–H) of $CH_3/CH_2$ group; stretching frequency of coordinated (C=O) that overlapped with other peaks like υ(C=N) which falls within this region; δ($CH_2$) [15]; {υ(C–N)+ υ(C–OH)} of primary amine and ethanol amine [31,32,39]; υ(Mn–OH) [40]; $\delta_r(CH_2)$ [15]; and υ(Mn–O) vibrations [40], respectively. Again, the last decomposition step observed in the temperature range (706-900°C) and (582-900°C) indicating to further ligand pyrolysis with the formation of ($Mn_3O_4$) and ($Co_3O_4$) as final products for Mn(II) and Co(II) complexes [56,60], individually, (Table 5). The final residue of the thermal decomposition of complexes (**1**) and (**2**) were explored by IR and XRD spectra. The IR spectra of the final products ($Mn_3O_4$) and ($Co_3O_4$) (Figs. 8b and 2b) show two bands at (614, 517$cm^{-1}$) and (649, 549 $cm^{-1}$) represented to **ν**(Mn–O) and **ν**(Co–O), respectively [61-65]. In $Co_3O_4$ residue, the band observed at 649 $cm^{-1}$ may be related to υ(Co–O) where $Co^{2+}$ is tetrahedrally coordinated, while, the band observed at 549 $cm^{-1}$ is assigned to the υ(Co–O) where $Co^{3+}$ is octahedrally coordinated. It is clear that the XRD diffractogram peaks of the final products for Mn(II) and Co(II) complexes are consistent with the data of the JCPDS cards number (24-0734) for ($Mn_3O_4$), (Fig. 7c) [66] and (01-076-1802) for $Co_3O_4$ (Fig. 10b), respectively. The X-ray patterns demonstrate that these oxides have a lower degree of crystallinity than their metal complexes. Figure (7c) showed broad and weak diffraction peaks for $Mn_3O_4$ residue due to its poor crystallinity or its small crystal particles. Its diffraction peaks are seen at 2θ

values of 33.84, 37.91, 42.35 and 71.08° indicating to the crystal planes of (103), (211), (400) and (321) of the tetragonal phase of $Mn_3O_4$ oxide, respectively, and they were similar to husmannite moiety $Mn_3O_4$ [63]. Also, Fig. 10b showed peaks at 2θ values of 22.01, 36.38, 43.05 and 65.69° correspond to the crystal planes of (111), (311), (400) and (440) of the cubic phase of $Co_3O_4$ oxide, respectively [64,65]. The average crystallite size of the final products was calculated using Debeys-Scherrer equation [22] to give diameters of 29.4, 42.05nm for $Mn_3O_4$ and $Co_3O_4$ oxides, respectively, indicating to nanonature for these oxides [63-65].

$$D=K\lambda/\beta Cos\theta$$

where D is the crystallite size, *K*= shape factor, with a value close to unity. The shape factor has a typical value of about 0.9, but varies with the actual shape of the crystallite; λ is the wavelength of X-ray, θ-angle diffraction and *β*-Full width at Half Maximum.

***Insert Figures (7-10) and their captions here***

$[Ni_2(L)Cl_4(H_2O)_2].5H_2O$ (**3**), $[Zn_2(L)Cl_4(H_2O)_2].7H_2O$ (**5**) complexes decompose in three stages but the decomposition of $[Cu_2(L)Cl_3(H_2O)_3].Cl.11H_2O$ (**4**) occurs in five steps. The first decomposition step within the temperature range (31-398$^o$C), (26-251$^o$C) and (25-333$^o$C) points to the elimination of outersphere water molecules (5, 7 and 3.5 $H_2O$); associated with TG weight losses (10.55, 12.58 and 6.69 %) for complexes (**3**), (**4**) and (5), respectively. This step is accompanied with weak to medium DTG peaks at $T_{max.}$= (52,306 $^o$C); (48,73,176 $^o$C) and (36$^o$C) for complexes (**3**), (**4**) and (**5**), respectively. This step follows first order of reaction for complexes (**3**), (**4**) and second order of reaction for complex (**5**) but, the calculated activation energy are (92.57, 225.23 KJmol$^{-1}$); (26.81, 123.71, 268.54 KJmol$^{-1}$) and (120.8 KJmol$^{-1}$) for complexes (**3**), (**4**) and (**5**), respectively. After that, the thermal decomposition process of complexes **(3)** and (**5**) occurs in the second and third steps at temperature ranges; (333-538°C) and (394-798$^o$C). The second one depicts TG weight losses (32.65 and 14.61%) corresponding to the partial ligand pyrolysis and partial dehalogenation along with release of the rest lattice water molecules associated with first and second kinetic order

for complexes (**3**) and (**5**), respectively, Tables (5 and 6). The third step at temperature range (394-798$^{o}$C) may be assigned to complete delegation together with dehalogenation and removal of coordinated water leading to the formation of 2NiO and 2ZnO as final products [11,12,67,68]. On the other hand, the TG curve of complex (**4)** displays weight loss (36.56, 10.51%) in the temperature range (251-445°C) corresponding to the removal of ($C_{21}H_{22}N_2$+$Cl_2$) with strong DTG peak at ($T_{max}$=307°C) in the second stage and release of two mole of coordinated $H_2O$ gathered with the rest of hydrated $H_2O$ in the third stage. The calculated order of reaction and activation energies were found (1.53, 146.23; 1.61, 317.46 KJmol$^{-1}$) for these steps. Then, complete delegation associated with the removal of chlorine gas takes place in the temperature range (445-630°C) resulting in 2CuO as a final product [68], Table 5. The nature of the solid products characteristic to complexes (**3**) and (**4**) was determined on the basis of the TG graphs and confirmed by their IR spectra (Figs. 3b and 4b) and X-ray diffraction (Figs. 11b and 12b). The diffractogram related to the final product NiO shows diffraction peaks at 2θ values of 37.45, 43.51, 58.59 and 74.7 indicating to the crystal planes of (111), (200), (220) and (311) matching with the standard values characteristic to pure cubic phase of NiO [69]. Also, this is consistent with JCPDS card number (00-78-0429) [69]. But, the XRD diffraction pattern of the final residue CuO demonstrates peaks at 2θ values of 35.12, 41.44, 45.35, 62.99 and 74.17° indicating to the crystal planes of (002), (1$^{-}$11), (200), (020) and (1$^{-}$13) of the monoclinic phase of CuO oxide, respectively [70,71]; this is confirmed with ASTM card number (01-089-5907) [70,71]. The average crystallite size of the final products was calculated using Debeys-Scherrer equation [22] to give diameters of 37.5 and 60.2 nm for NiO and CuO oxides, respectively. Moreover, Figs 3b and 4b showed peaks at 674, 491, 435 and 660, 520 cm$^{-1}$ assigned to υ(Ni–O) and υ(Cu–O) of NiO and CuO [69-71], respectively.

***Insert Figures (11-13) and their captions here***

In order to demonstrate the effects of the structural properties of the metal complexes and the type of the metal ion on the thermal behavior of them, the values of activation energy $\Delta E^*$ and the order of the reaction for the various decomposition stages were calculated and discussed through the analysis of the DTG curves. Some remarks and conclusions were obtained using the TG/DTG curves and kinetic parameters, as follows:

- Ni(II) complex (**3**) has higher thermal stability (369°C) than the corresponding for Mn(II), Co(II) and Zn(II) complexes, this is may be due to the lower ionic radii of Ni(II) ion than the others [47,72]. Moreover, the activation energy value of complexes increases as the thermal stability increases. So, $\Delta E^*$ value for the initial decomposition for Ni(II) complex (**3**) is higher than that the corresponding $\Delta E^*$ for complex (**1, 2, 5**), Table (6).
- All the decomposition processes of all metal complexes proceed through first order reaction except Zn(II) complex where its decomposition processes proceeds through first and second order reaction, (Table 6). Also, the fraction appeared in the calculated order of the thermal reactions (n), confirmed that the reactions proceeded in complicated mechanisms [73,74].
- The change of entropy values ($\Delta S^*$) of complexes **(1-5)** for the thermal decompositions stages (Table 6), illustrated that the transition states are more ordered, than the reacting complexes [73,74].

**3.7. Powder XRD studies**

The X-ray diffraction patterns of metal complexes (**1-5)** are shown in Figs. (7a, 10a, 11a, 12a and 13). The spectra showed sharp crystalline peaks indicating to their crystalline nature. The average crystallite size of the complexes was calculated using Debeys-Scherrer equation [22]. Using the full width at half maximum intensity of the peaks, the average sizes are found to be 34.68, 31.31, 21.73, 18.66 and 27.99 nm for complexes (**1**), (**2**), (**3**), (**4**) and (**5**), respectively, indicating to nanostructure for these compounds.

***Insert Table 5 and its caption here***

***Insert Table 6 and its caption here***

### 3.8. Electronic Spin Resonance (ESR) Spectral Studies

ESR spectra of Cu(II) complex (**4**) were recorded at room temperature as polycrystalline samples, on X-band at frequency of 9.71 GHz. The spectral analyses of complex (**4**) give $g_{//}$ = 2.269, $g\perp$ = 2.073 and G = 3.77. The observed $g_{//}$ value for complex (**4**) is less than 2.3 in agreement with the covalent character of the metal ligand bond. The trend $g_{//} > g\perp > 2.0023$ observed for this complex, indicates that unpaired electron is localized in $d_{x2-y2}$ orbital of the Cu(II) ion and the spectral features are characteristic of axial symmetry [68,75]. Thus, a tetragonal geometry is confirmed for the aforesaid complex [15,76]. $G = (g_{//} - 2.0023) / (g\perp - 2.0023)$, which measures the exchange interaction between the metal centers in a polycrystalline solid, has been calculated. According to Hathaway, if $G > 4$, the exchange interaction is negligible, but $G < 4$ indicates considerable exchange interaction in the solid complexes [77]. The G value for complex (**4)** is slightly less than 4, indicating the exchange interaction in solid complex.

### 3.9.1. Biological Activity

The present results revealed that *Eobania vermiculata* was comparatively less susceptible to MDA and complexes (**1-4**) than *Monacha obstructa* which was less susceptible to complex (**5**) than *Eobania vermiculata*. Reviewing the above mentioned results, it is obvious that there are different susceptibility levels between the two tested snail species according to type of tested compound. These differences in the sensitivity levels may be due to the physiological state of the snail which changes from species to another [15,78]. The data represented in Table (7) concluded that:

1- MDA has higher toxicity than the metal complexes against the two land snail species. This is may be attributed to the presence of free amino groups in the former which can react in cells leading to the initiation of carcinogenic process [79].

2- Copper(II) complex (**4**) has higher toxicity against the two land snails than other complexes. This is may be ascribed to the higher toxicity of Cu(II) ions [80] which facilitate the entrance into the snail cell wall and exert metal toxic action on the metabolic activity of snails.

***Insert Table 7 and its caption here***

### 3.9.2. Cytotoxicity assay

The synthesized compounds (**1-5**) were screened *in vitro* against human-hepatic carcinoma cell line, Hep-G2 using doxorubicin (DOX) as a reference drug. Cytotoxicity of doxorubicin on Hep-G2 was assessed using calorimetric method. The results were compared to the antiproliferative effects of the reference control doxorubicin as shown in Table 8, plotted in Figure 14. Responses of Hep-G2 cells toward increase concentrations of metal complexes were exponential. Hep-G2 cells experienced a significant increase in viability at low concentrations of metal complexes, with an eventual decline at the highest concentrations tested. The estimated $IC_{50}$ values ranged between 41.9 and 7.09 *μg/ml* after 24 hours. From the results (Table 8), it is evident that all the tested complexes displayed moderate growth inhibitory activity, in particular compounds (**5**), (**3**) and **(2)** ($IC_{50}$ 7.09, 9.11 and 10.7 *μg/ml*), respectively. The antiproliferative activity of the test compounds against HepG2 cell line may be arranged in order Zn, Ni, Co, Mn, Cu {i.e. (**5**) > (**3**) > (**2**) > (**1**) > (**4**)} which corresponds to the concentration required for 50% inhibition of cell viability.

***Insert Figure (13) and its caption here***

***Insert Table (8) and its caption here***

## 4. Conclusion

In this work, the newly Mn(II), Co(II), Ni(II), Cu(II) and Zn(II) complexes with Schiff base were prepared by template condensation reaction of 4,4'-methylenediamine, benzile and ethanolamine. They are confirmed via various methods of analysis. The results obtained can be summarized as following:

(1) This work suggested that the formed HL behaves as monoanil asymmetric moiety and chelating neutral tetradentate ligand in all metal complexes, bonding with the metal ion occurs through azomethine nitrogen, $NH_2$ group nitrogen atoms and oxygen atom of ethanolamine OH group. All complexes were found to be binuclear.

(2) The IR spectra elucidated that one mole of benzile and one mole of ethanolamine are involved in condensation with only one $NH_2$ group of MDA but the other mole of EA used as adduct in metal complexes.

(3) The data showed that all complexes are non-electrolytes except Cu(II) complex. Electronic spectra, of metal complexes display octahedral stereochemistry which is confirmed by magnetic moments at room temperature.

(4) The ESR spectra for Cu(II) complex showed axially symmetric g-tensor parameter with $g_{//} > g_{\perp} > 2.0023$ demonstrating to $^2B_{1g}$ ground state with $(d_{x2-y2})^1$ configuration.

(5) The thermal decomposition of metal complexes was investigated by TG analysis within temperature range 26-900°C, resulting in the formation of metal oxide as end products as both IR spectra and X-ray diffraction indicates. In addition, the thermodynamic parameters of the dissociation steps were calculated from DTG curves.

(6) The powder X-ray diffraction patterns indicate that all metal complexes have a nanostructure.

(7) The biological activity of the synthesized metal complexes was studied against two Land Snails, the glassy clover snail *Monacha obstructa* and the brown garden snail, *Eobania vermiculata* and also, against human-hepatic carcinoma cell line, Hep-G2. It was found that Cu(II) complex has higher toxicity against the two land snails than other complexes. Additionally, Zn(II) complex (**5**), exhibits a high inhibition of growth of the cell line with $MIC_{50}$ of 7.09 *μg/mL*.

**References**

[1] M.N. Uddin, Md. A. Salam, J. Sultana, Pb(II) Complexes of Schiff bases derived from benzoylhydrazine as the antibacterial agents, Mod. Chem. 3 (2015) 7-14.

[2] (a) X. Zhou, L. Shao, Z. Jin, J.-B. Liu, H. Dai, J.-X. Fang, Synthesis and antitumor activity evaluation of some Schiff bases derived from 2-aminothiazole derivatives, Heteroat. Chem. 18 (2007) 55-59; (b) H.A. Saadeh, E.A. Abu Shaireh, I.M. Mosleh, A.G. Al-Bakri, M.S. Mubarak, Synthesis, characterization and biological activity of Schiff bases derived from metronidazole, Med. Chem. Res. 21 (2012) 2969–2974.

[3] X.F. Luo, X. Hu, X.Y. Zhao, S.H. Goh, X.D. Li, Miscibility and interactions in blends and complexes of poly(4-methyl-5-vinylthiazole) with proton-donating polymers, Polymer 44 (2003) 5285-5291.

[4] C.K. Bhkahk, J.S. Hadi, New unsymmetrical Schiff base as inhibitor of carbon steel corrosion and antibacterial activity, Res. J. Chem. Sci. 5 (2015) 64-70.

[5] A.K. Gupta, R. Pal, Dehydroacetic acid based Schiff's bases and their metal complexes: a review, World J. Pharm. Pharm. Sci. 4 (2015) 386-425.

[6] I.R. Parrey, A.A. Hashmi, Synthesis of Schiff base complexes of Mn(II) and Co(II) and their catalytic oxidation towards olefins and alcohols, Can. Chem. Trans. 3 (2015) 65-71

[7] P.J.E. Quintana, A. de Peyster, S. Klatzke, H.J. Park, Gossypol-induced DNA breaks in rat lymphocytes are secondary to cytotoxicity, Toxicol. Lett. 117 (2000) 85–94

[8] (a) G. Yadav, J.V. Mani, Green synthesis of Schiff bases by using natural acid catalysts, Int. J. Sci. Res. 4 (2015) 121-127; (b) C. Maxim, T.D. Pasatoiu, V. Ch. Kravtsov, S. Shova, C.A. Muryn, R.E.P. Winpenny, F. Tuna, M. Andruh, Copper(II) and zinc(II) complexes with Schiff-base ligands derived from salicylaldehyde and 3-metoxysalicylaldehide: synthesis, crystal structures, magnetic and luminescence properties, Inorg. Chim. Acta 361 (2008) 3903-3911.

[9] I.J. Patel, S.J. Parmar, Synthesis and studies of novel optically active Schiff's base derivatives and their antimicrobial activities, E.-J. Chem. 7 (2010) 617-623.

[10] N. Charef, F. Sebti, L. Arrar, M. Djarmouni, N. Boussoualim, A. Baghiani, S.

Khennouf, A. Ourari, M.A. AlDamen, M.S. Mubarak, D.G. Peters, Synthesis, characterization, X-ray structures, and biological activity of some metal complexes of the Schiff base 2,2'-(((azanediylbis(propane-3,1-diyl))bis(azanylylidene))bis(meth-anylylidene))diphenol, Polyhedron 85 (2015) 450–456

[11] V.P. Singh, P. Gupta, N. Lal, Synthesis, spectral, and biological studies of some metal(II) complexes with benzil salicylaldehyde acyldihydrazones, Russ. J. Coord. Chem. 34 (2008) 270-277.

[12] A. M. Abu-Dief, I.M.A. Mohamed, A review on versatile applications of transition metal complexes incorporating Schiff bases, Beni-Suef Univ. J. Basic Appl. Sci. 4 (2015) 119-133.

[13] L. Chiang, M. R. Jones, C. L. Ferreira, T. Storr, Multifunctional ligands in medicinal inorganic chemistry- current trends and future directions, Curr. Topics Med. Chem. 12 (2012) 122-144.

[14] T. Storr, K. H. Thompsona, C. Orvig, Design of targeting ligands in medicinal inorganic chemistry, Chem. Soc. Rev. 35 (2006) 534-544.

[15] S.A. AbouEl-Enein, S.M. Emam, M.W. Polis, E.M. Emara, Synthesis and characterization of some metal complexes derived from azo compound of 4,4'-methylenedianiline and antipyrine: Evaluation of their biological activity on some land snail species, J. Mol. Struct. 1099 (2015) 567-578.

[16] P. Botella, A. Corma, R.H. Carr, C.J. Mitchell, Towards an industrial synthesis of diamino diphenyl methane (DADPM) using novel delaminated materials: A breakthrough step in the production of isocyanates for polyurethanes, Appl. Catal. A: General 398 (2011) 143-149.

[17] I. Alan, A. Kriza, M. Badea, N. Stanical, R. Olar, Synthesis and characterization of Co(II), Ni(II), Zn(II) and Cd(II) complexes with 5-bromo-N,N'-bis-(salicylidene)-o-tolidine, J. Therm. Anal. Calorim. 111 (2013) 483-490.

[18] M. Mizunoa, K. Iwata, H. Takahashi, Time-resolved infrared and resonance

raman studies of benzyl, vibrational analysis and structures of the excited states, J. Mol. Struct. 661-662 (2003) 3–10.

[19] D. Singh, K. Kumar, R. Kumar, J. Singh, Template synthesis and characterization of biologically active transition metal complexes comprising 14-membered tetraazamacrocyclic ligand, J. Serb. Chem. Soc. 75 (2010) 217–228.

[20] J. Bassett, R.C. Denney, G.H. Jeffery, J. Mendham, Vogel's Textbook of Quantitative Inorganic Analysis Including Elementary Instrumental Analysis, 4th ed., Longman Group, London, (1978); (#) Note: The halide content in the complexes was indirectly determined by Mohr's method after the decomposition of the samples in concentrated nitric acid by boiling, followed by addition of distilled $H_2O$ to give aqueous solution of metal salt.

[21] J. Lewis, R.G. Wilkins, Modern coordination chemistry, Interscience, New York, (1960) p. 403.

[22] M.V. Kumar, S. Muthulakshmi, A. A. Paulfrit, J. Pandiarajan, N. Jeyakumaran, N. Pandiarajan, Structural and optical behavior of thermally evaporated *p*-type nickel oxide thin film for solar cell applications, Inter. J. Chem Tech Res.13 (2014) 5174-5177.

[23] A. Monks, D. Scudiero, P. Skehan, R. Shoemaker, K. Paull, D. Vistica, C. Hose, J. Langley, P. Cronise, A. Vaigro-Wolff, M. Gray-Goodrich, H. Campbell, J. Mayo, M. Boyd, Feasibility of a high-flux anticancer drug screen using a diverse panel of cultured human tumor cell lines, J. Nat. Cancer Institute 83 (1991) 757–766.

[24] (a) A.A. Mourad, Molluscicidal effect of some plant extracts against two land snail species, Monacha obstructa and Eobania vermiculata, Egypt. Acad. J. Biolog. Sci. 6 (2014) 11-16; (b) R.S. Ascher, F. Mirian, The residual contact toxicity of Bay Sir 8514 to Spodoptera littoralis Larva, Phytoparasitica 9 (1981) 133-137.

[25] D.J. Finney, Probit Analysis, 3rd ed., Cambridge University Press, London

(1971) p. 318.

[26] S. Saikat, N.S. Kumar, C.A. Prasun, D. Kamalendu, Synthesis and spectroscopic characterization of some iron(III) complexes with tetradentate Schiff base ligands, Ind. J. Sci. 12 (2015) 17-24.

[27] A.M. Khedr, F.A. Saad, Synthesis, structural characterization, and antimicrobial efficiency of sulfadiazine azo-azomethine dyes and their bi-homonuclear uranyl complexes for chemotherapeutic use, Turk. J. Chem. (2015) 1-14

[28] F.A. Al-Saif, Spectroscopic elucidation, conductivity and activation thermodynamic parameters studies on Pt(IV), Au(III) and Pd(II) 1,5-dimethyl-2-phenyl-4-[(thiophen-2-ylmethylene)-amino]-1,2-dihydro-pyrazol-3-one Schiff base complexes, Int. J. Electrochem. Sci. 9 (2014) 398 – 417.

[29] A. Mahal, R. Abu-El-Halawa, S.A. Zabin, M. Ibrahim, M. Al-Refai, T. Kaimari, Synthesis, characterization and antifungal activity of some metal complexes derived from quinoxaloylhydrazone, World J. Org. Chem. 3 (2015) 1-8.

[30] S.A. AbouEl-Enein, Polymeric and sandwich Schiff's bases complexes derived from 4,4'-methylenedianiline; characterization and thermal investigation, J. Therm. Anal. Calorim. 91 (2008) 929–936.

[31] H. M. Badawi, A comparative study of the structure and vibrational spectra of diphenylmethane, the carcinogen 4,4′-methylenedianiline and 4,4′-methylenebis-(N,N-dimethylaniline), Spectrochim. Acta A 109 (2013) 213–220.

[32] M. Shebl, Synthesis, spectral and magnetic studies of mono- and bi-nuclear complexes of a new bis(tridentate $NO_2$) Schiff base ligand derived from 4,6-diacetylresorcinol and ethanolamine, Spectrochim. Acta A 73 (2009) 313–323.

[33] A. Jha, Y.L.N. Marthy, G. Durga, Synthesis, characterization and bioactivity of transition metal complexes of new 3-methyl-5-mercapto-4-triazole Schiff bases, Res. J. Pharm. Biol. Chem. Sci. 6 (2015) 1306-1314.

[34] P.Karthikeyan, S.A.Aswar, P.N.Maskawar, P.R.Bhagat, S.S.Kumar, Development and efficient 1-glycyl-3-methylimidazolium chloride copper(II)

complex catalyzed highly enantioselective: synthesis of 3,4-dihydropyrimidin-2|(1H)-ones, J. Organom. Chem. 723 (2013) 154-162.

[35] A.C. Tella, J.A.Obaleye, Copper(II) complexes of 4,4'-diaminodiphenylsulphone: Synthesis, characterization and biological studies, E.-J. Chem. 6 (2009) 5311-5323.

[36] D.S. Kumar, S.R. Gandhi, A.K.I. Sheriff, Synthesis, spectral characterization and antimicrobial activity of bidentate Schiff's base ($N_2$) transition metal complexes, J. Chem. Pharm. Res. 7 (2015) 416-423.

[37] B. Stuart, Infrared spectroscopy: Fundamentals and applications, John Wiley & Sons, (2004).

[38] M.S. Masoud, A. El-Marghany, A. Orabi, A.E. Ali, R. Sayed, Spectral, coordination and thermal properties of 5-arylidene thiobarbituric acids, Spectrochim. Acta A 107 (2013) 179–187

[39] M. Rezaeivala, R. Golbedaghi*b*, M. Khalili, Coordination Chemistry of Some New Cu(II), Ni(II) and Co(II) Macroacyclic ($N_2O_4$) Schiff Base Complexes: X-ray Crystal Structure of Cu(II) Complex, Russ. J. Coord. Chem. 42 (2016) 66–70.

[40] G. Pethe, A. Yaul, A. Aswar, Synthesis, spectroscopic and thermal studies of some complexes of unsymmetrical Schiff base ligand, J. Therm. Anal. Calorim. 107 (2012) 97-103.

[41] P. Tyagi, S. Chandra, B.S. Saraswat, Ni(II) and Zn(II) complexes of 2-((thiophene-2-ylmethylene)amino)benzamide: synthesis, spectroscopic characterization, thermal, DFT, and anticancer activities, Spectrochim. Acta A 134 (2015) 200-209.

[42] A.H. Khan, A. Bashar, U. Shingh, M.M. Dar, A.A. Hashmi, Synthesis, characterization and antimicrobial activity of metal complexes with diethanolamine and nitro ligands, Eur. Acad. Res. 8 (2014) 10714–10724.

[43] M**.** Zimmer, Bioinorganic Molecular Mechanics, Chem. Rev. 95 (1995) 2629-

2649.

[44] B.P. Hay, R.D. Hancock , The role of donor group orientation as a factor in metal ion recognition by ligands Review Article, Coord. Chem. Rev. 212 (2001) 61-78.

[45] S.M. Emam, I.E. El sayed, N. Nassar, Transition metal complexes of neocryptolepine analogues, Part I: Synthesis, spectroscopic characterization and in vitro anticancer activity of copper(II) complexes, Spectrochim. Acta A 138 (2015) 942-953.

[46] M. Salavati-Niasari, F. Davar, K. Saberyan, Template synthesis and characterization of diazadioxa macrocyclic nanosized cobalt(II) complex dispersed within nanocavity of zeolite-Y, Polyhedron 29 (2010) 2149-2156.

[47] A.Z. El-Sonbati, A.A. Diab, A.A. El-Bindary, A.M. El-Desoky, Sh.M. Morgan, Correlation between ionic radii of metals and thermal decomposition supramolecular structure of azodye complexes, Spectrochim. Acta A 135 (2015) 774-791.

[48] F.A. El-Saied, S.A. AbouEl-Enein, S.M. Emam, H.A. El-Shater, Synthesis and characterization of Cu(II), Ni(II), Co(II), Mn(II), Zn(II), Ru(III), Hf(IV) and ZrO(II) complexes of 2-thiophenylidene-N-4-methoxy anilinoacetohydrazone, Polish J. Chem. 83 (2009) 1871–1883.

[49] S.M. Emam, S.A. AbouEl-Enein, F.A. El-Saied, S.Y. Alshater, Synthesis and characterization of some bi, tri and tetravalent transition metal complexes of N'-(furan-2-yl-methylene)-2-(p-tolylamino)acetohydrazide $HL^1$ and N'-(thiophen-2-yl-methylene)-2-(p-tolylamino)acetohydrazide $HL^2$, Spectrochim. Acta A 92 (2012) 96–104.

[50] S.M. Emam, A.S. El-Table, H.M. Ahmed, E.A. Emad, Synthesis, structural characterization, electrochemical and biological studies on divalent metal chelates of a new ligand derived pharmaceutical preservative: dehydroacetic acid with 1,4-diaminobenzene, Arab. J. Chem. xx (2014) xxx. In Press.

[51] S.K. Tripathy, A. Panda, P.K. Das, N.K. Behera, A. Mahapatra, A.K. Panda, Homo and bimetallic dinuclear macrocyclic complexes of 1,4,5,8,11,14,15,18,19,21-decaaza-2,3,6,7,12,13,16,17-octaphenyl-20-thia-undodecane1,3,5,7,11,13,15,17-octaene (dotuo): Its synthesis, characterization and biological properties, Int. J. Sci., Environ. Technol., 3 (2014) 208–223.

[52] Z.H. Chohan, M. Arif, M.A. Akhtar, C.T. Supran, Metal-based antibacterial and antifungal agents: synthesis, characterization, and in vitro biological evaluation of Co(II), Cu(II), Ni(II) and Zn(II) complexes with amino acid-derived compounds, Bioinorg. Chem. Appl. (2006) 1-13.

[53] A.S. El-Tabl, S. AbouEl-Enein, Reactivity of the new potentially binucleating ligand, 2-(acetichydrazido-*N*-methylidene-α-naphthol)-benzothiazol, towards manganese(II), nickel(II), cobalt(II), copper(II) and zinc(II) salts, J. Coord. Chem. 57 (2004) 281-294.

[54] Z. B. Leka, V.M. Leovac, S. Lukić, T. J. Sabo, S.R. Trifunović, K.M. Szécsényi, Synthesis and physicochemical characterization of new dithiocarabamato ligand and its complexes with copper(II), nickel(II) and palladium(II), J. Therm. Anal. Calorim. 83 (2006) 687-691.

[55] T. Rosu, E. Pahontu, C. Maxim, R. Georgescu, N. Stanica, G.L. Almajan, A. Gulea, Synthesis, characterization and antibacterial activity of some new complexes of Cu(II), Ni(II), VO(II), Mn(II) with Schiff base derived from 4-amino-2,3-dimethyl-1-phenyl-3-pyrazolin-5-one, Polyhedron 29 (2010) 757-766.

[56] H.A. El-Boraey, S.M. Emam, D.A. Tolan, A.M. El-Nahas, Structural studies and anticancer activity of a novel ($N_6O_4$) macrocyclic ligand and its Cu(II) complexes, Spectrochim. Acta A 78 (2011) 360–370.

[57] O.P. Gupta, A. Kumar, Metal complexes as ligand: binuclear Ni(II) and Cu(II) metal chelates of p-methylisonitrosoacetophenone with alkali metal salts, J. Chem. Chem. Sci. 5 (2015) 69-78.

[58] G.O. Piloyan, I.D. Ryabchikov, O.S. Novikova, Nature 212 (1966) 1229.

[59] Y. Kirsh, S. Yariv, S. Shoval, J. Therm. Anal. Calorim. 32 (1987) 393-408.

[60] A.M.A. Alaghaz, M.E. Zayed, S.A. Alharbi, R.A.A. Ammar, J. Mol. Struct. 1087 (2015) 60-67.

[61] M. Salavati-Nasari, M. Farhadi-Khouzani, F. Davar, Bright blue pigment $CoAl_2O_4$ nanocrystals prepared by modified sol-gel method, J. Sol-Gel Sci Technol. 52 (2009) 321-327.

[62] S. Farhadi, J. Safabakhsh, P. Zaringhadam, Synthesis, characterization, and investigation of optical and magnetic properties of cobalt oxide ($Co_3O_4$) nanoparticles, J. Nanostru. Chem. 3 (2013) 1-9.

[63] Z. Bai, B. Sun, N. Fan, Z. Ju, M. Li, L. Xu, Y. Qian, Branched mesoporous $Mn_3O_4$ nanorods: Facile synthesis and catalysis in the degradation of methylene blue, Chem. Eur. J. 18 (2012) 5319-5324.

[64] O. Stefanescu, T. Vlase, S. Sorescu, P. Barvinschi, M. Stefanescu, Thermal behavior of Co(II) and Ni(II) by hydroxycarboxylate complexes obtained by two original synthesis methods, J. Therm. Anal. Calorim. 113 (2013) 1345-1354.

[65] Z. Durmurs, H. Kavas, A. Baykal, M.S. Topark, A green chemical route for the synthesis of $Mn_3O_4$ nanoparticles, Cent. Eur. J. Chem. 7 (2009) 555-559.

[66] J. Du, Y. Gao, L. Chai, G. Zou, Y. Li, Y. Qian, Hausmannite $Mn_3O_4$ nanorods: synthesis, characterization and magnetic properties, Nanotechnology 17 (2006) 4923-4928

[67] L.Calu, M.Badea, D.Falcescu, D.Duca, D.Marinescu, R.Olar, Thermal study on complexes with Schiff base drived from 1,2,4-triazole as potential antimicrobial agents, J. Therm. Anal. Calorim. 111(2013) 1725–1730.

[68] J.R. Anacona, N. Noriega, J. Camus, Synthesis, characterization and antibacterial activity of a tridentate Schiff base derived from cephalothin and sulfadiazine, and its transition metal complexes, Spectrochim. Acta A 137 (2015) 16-22.

[69] M. Salavati-Niasari, N, Mir, F. Davar, Synthesis and characterization of NiO nanoclusters via thermal decomposition, Polyhedron 28 (2009) 1111-1114.

[70] G. Dzido , M. Drzazga, P. Markowski , Andrzej B. Jarzębski, Application of sonication and microwave irradiation to boost continuous fabrication of the copper(II) Oxide sub-micron particles, Technologies 3 (2015) 37-46.

[71] M. Orojloo, F. Nourian, R. Arabahmadi, S. Amani, Ni(II), Cu(II), AND Zn(II) Complexes derived from a new Schiff base 2-((*Z*)-(3-methylpyridin- 2-yleimino)methyl)phenol and synthesis of nano sized metal oxide particles from these compounds, Quim. Nova, 38 (2015) 1187-1191.

[72] Breviglieri ST, Cavalheiro ETG, Chierice GO. Correlation between ionic radius and thermal decomposition of Fe(II), Co(II), Ni(II), Cu(II) and Zn(II) diethanoldithiocarbamates, Thermochim. Acta 2000; 356:79-84.

[73] Masoud MS, Abou El-Enein SA, Ramadan AM, Goher AS. Thermal properties of some biologically active 5-(*p*-substituted phenylazo)-6-aminouracil complexes, J. Anal. Appl. Pyrol. 2008; 81: 45–51.

[74] Masoud MS, Ali AE, Ghareeb DA, Nasr NM. Structural, spectral and thermal analysis of some metallocephradine, J. Mol. Struct. 2015; 1099: 359–372.

[75] P. Tyagi, S. Chandra, B.S. Saraswat, D. Yadav, Design, spectral characterization, thermal, DFT studies and anticancer cell line activities of Co(II), Ni(II) and Cu(II) complexes of Schiff bases derived from 4-amino-5-(pyridin-4-yl)-4*H*-1,2,4-triazole-3-thiol, Spectrochim. Acta A 145 (2015) 155–164.

[76] S. Chandra, S. Bargujar, R. Nirwal, N. Yadav, Synthesis, spectral characterization and biological evaluation of copper(II) and nickel(II) complexes with thiosemicorbazone derived from a bidentate Schiff base, Spectrochim. Acta A 106 (2013) 91-98.

[77] B.J. Hathaway, J.N. Bardley, R.D. Gillard (Eds.), Essays in Chemistry,

Academic Press, New York, NY, USA, 1971.

[78] D. Godan. Pest slugs and snails, biology and control, Springer-verlag, Berlin Heidelberg, New York (1983).

[79] M.C. Garrigós, F. Reche, M.L. Marín, A. Jiménez, Determination of aromatic amines formed from azo colorants in toy products, J. Chromatogr. A 976 (2002) 309-317.

[80] K.S. El-Gendy, M.A. Radwan, A.F. Gad, In vivo evaluation of oxidative stress biomarkers in the land snail, Theba pisana exposed to copper-based pesticides, Chemosphere 77 (2009) 339–344.

# Figures

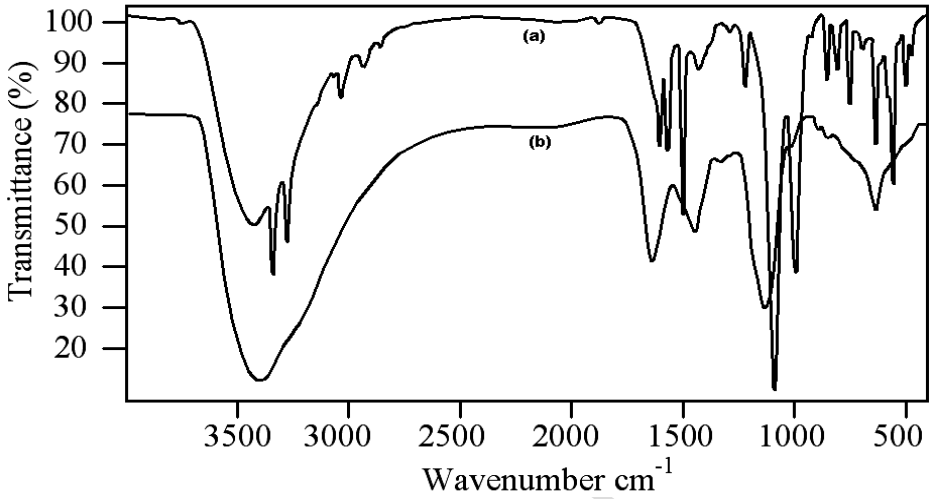


**Fig. 1** (a)IR spectra of $[Mn_2(L)Cl_4(H_2O)_2].7.5H_2O.0.5EtOH$.complex (**1**), before heating and (b) after heating up to 391°C

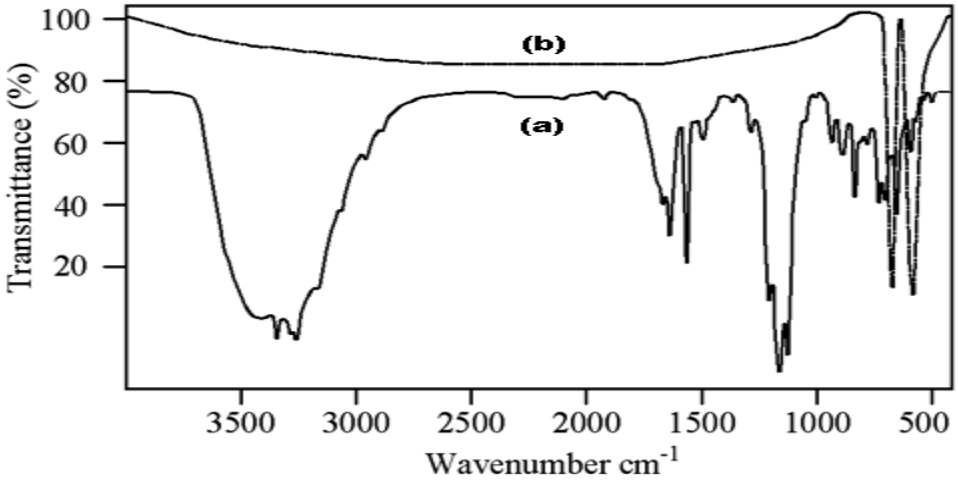


**Fig.2** (a) IR spectra of $[Co_2(L)Cl_4(H_2O)_2].8.5H_2O$ complex **(2)**,and (b) IR spectrum of final product ($Co_3O_4$) isolated fro

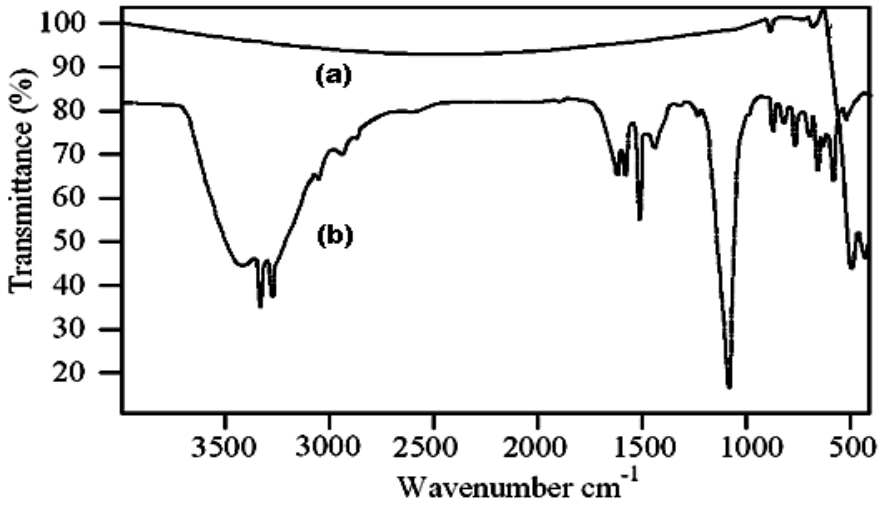


**Fig.3** (a) IR spectra of $[Ni_2(L)Cl_4(H_2O)_2].5H_2O$ complex **(3)**, (b) IR spectrum of final product (NiO) isolated from the thermal decomposition of Ni(II) complex up to 900°C

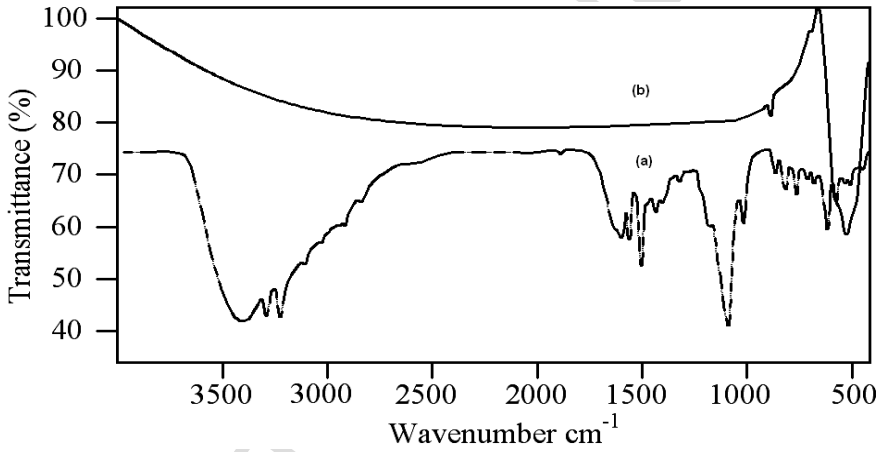


**Fig.4** (a) IR spectra of $[Cu_2(L)Cl_3(H_2O)_3].Cl.11H_2O$ complex **(4)**, (b) IR spectrum of a final product (CuO) isolated from the thermal decomposition of Cu(II)complex up to 900°C

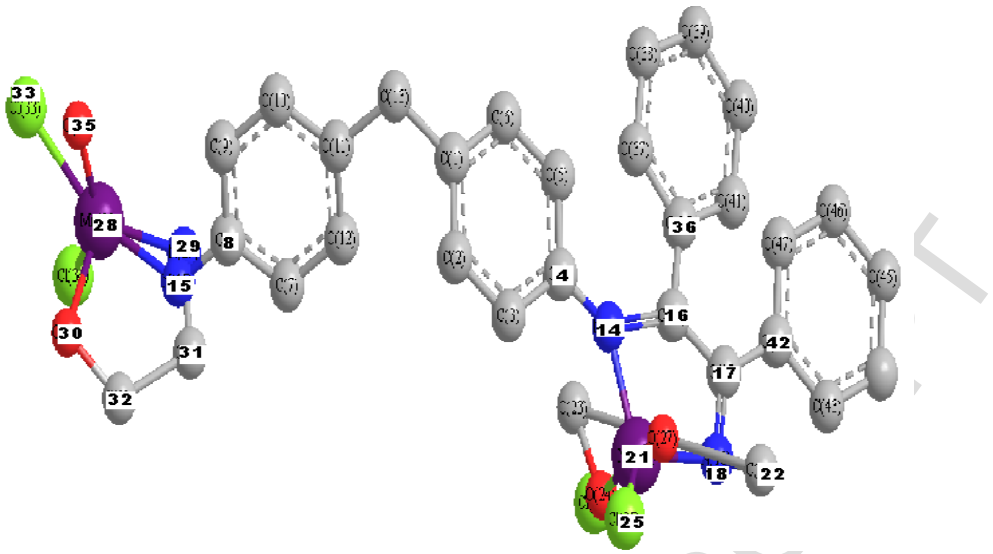


**Fig.5** Molecular modeling of Mn(II) complex (**1**) $[Mn_2(L)Cl_4(H_2O)_2].7.5H_2O.0.5EtOH$

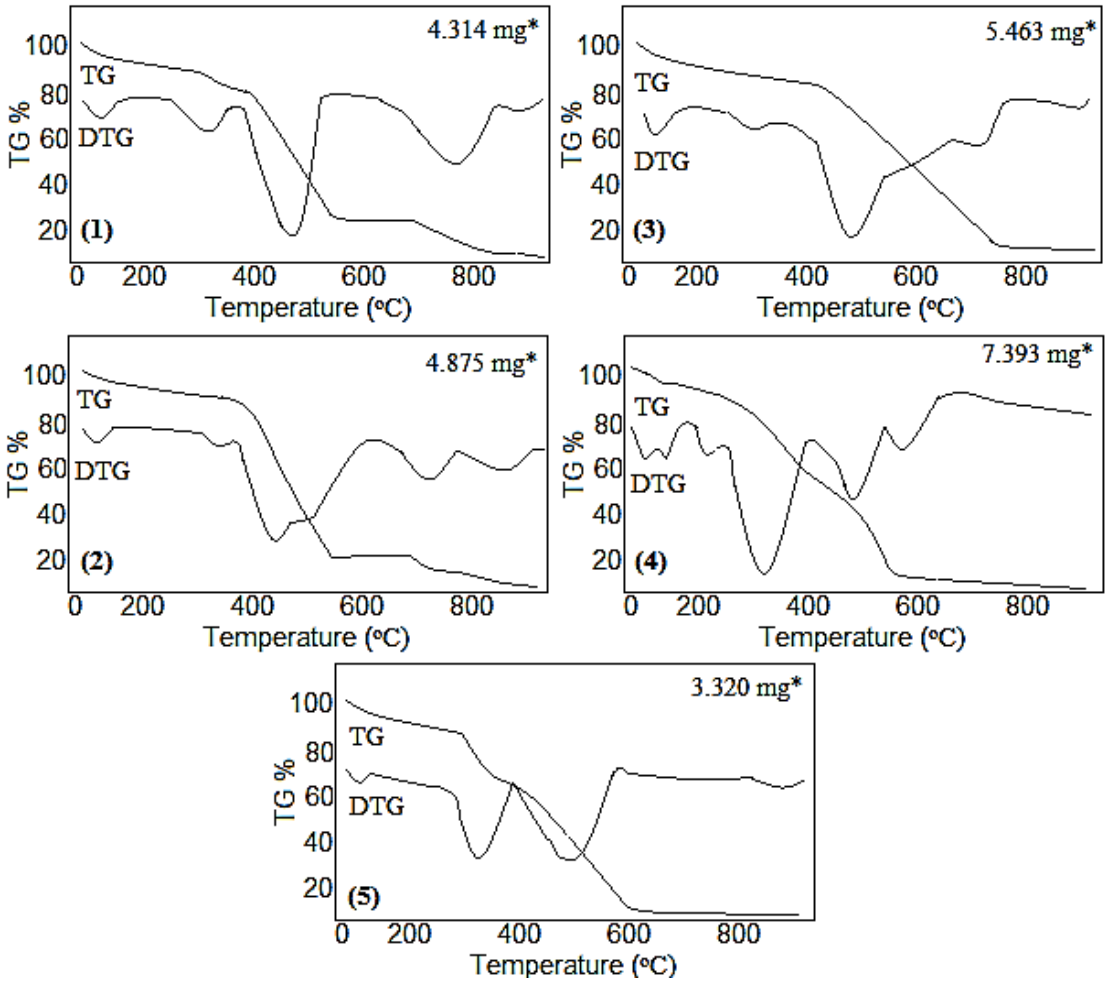


**Fig.6** TG/DTG curves for metal(II) complexes

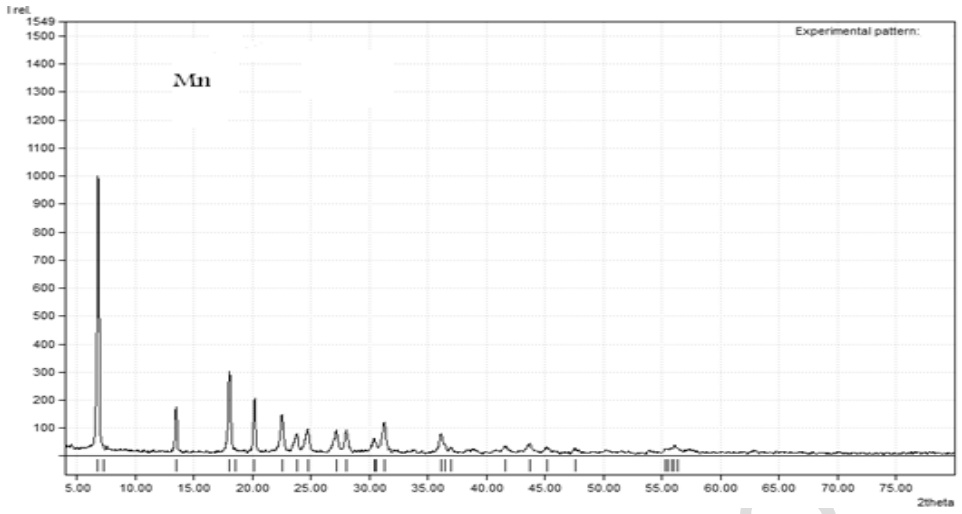


**Fig.7** (a) XRD pattern of manganese(II) complex (**1**)

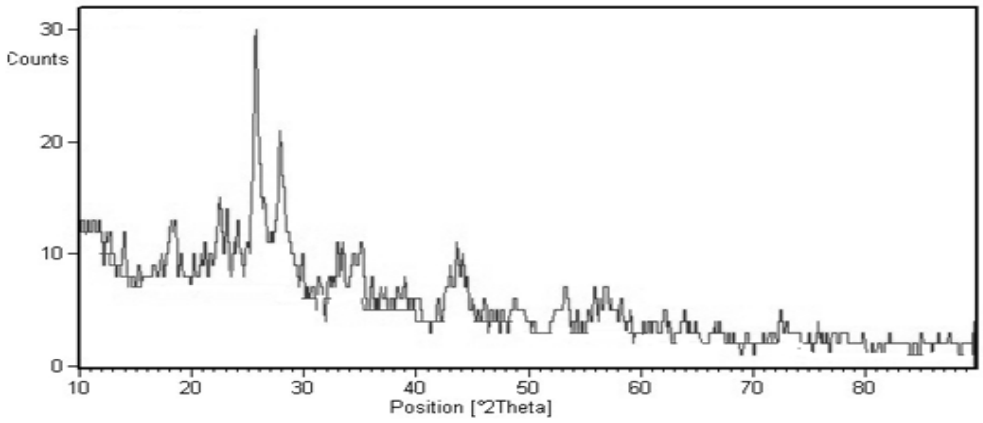


**Fig.7** *Continued* (b) XRD pattern of Mn(II) complex, (**1**) after heating up to 391°C (desolvation step)

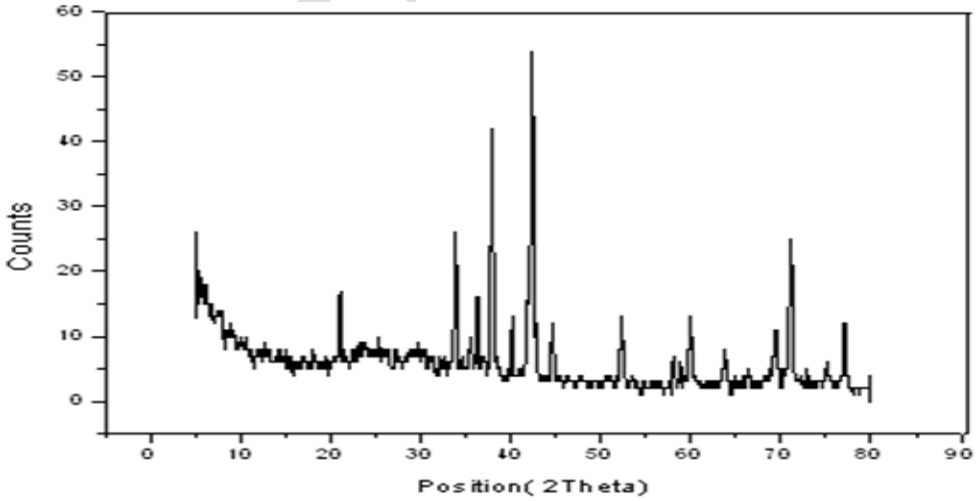


**Fig.7** *Continued* (c) XRD pattern of solid residue ($Mn_3O_4$), resulted from the thermal decomposition of Mn(II) complex(**1**) up to 900°C

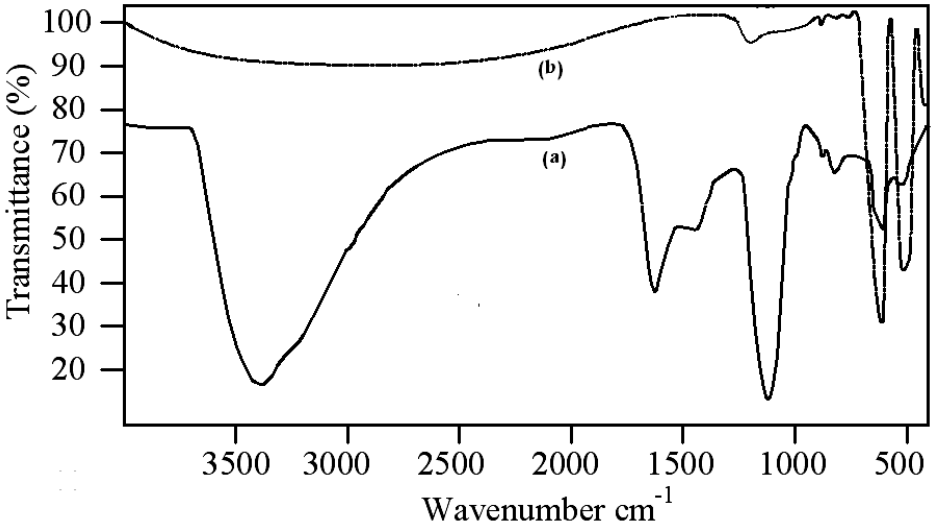


**Fig. 8** (a) IR spectrum of intermediate isolated from heating of complex **(1)** up to 538°C and (b) IR spectrum of final product ($Mn_3O_4$) isolated from the thermal decomposition of complex **(1)** up to 900°C

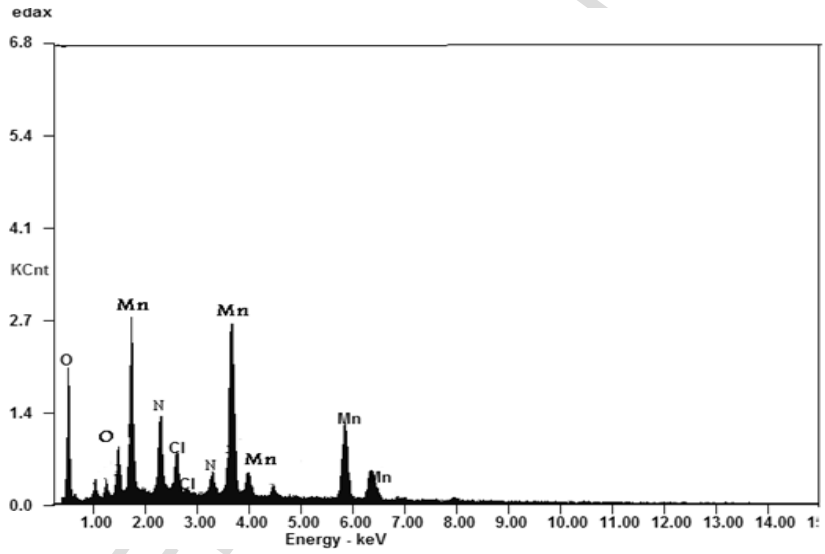


**Fig. 9** EDX of intermediate isolated from heating of Mn(II) complex **(1)** up to538°C

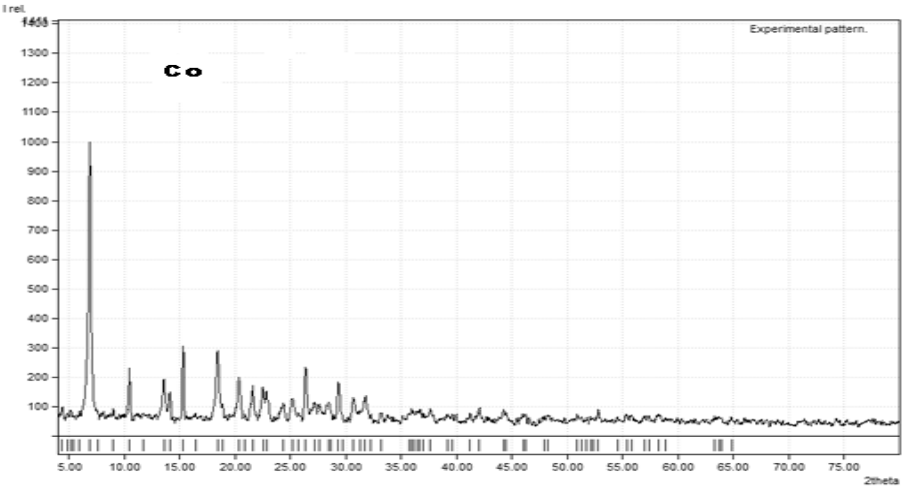


**Fig.10** (a) XRD pattern of cobalt(II) complex (**2**)

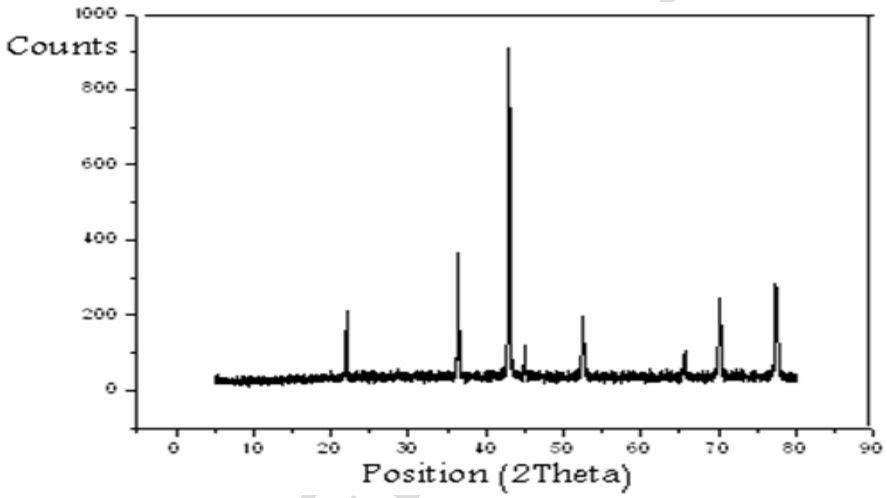


**Fig.10** *Continued* (b) XRD pattern of solid residue ($Co_3O_4$), resulted from the thermal decomposition of Co(II) complex (**2**)

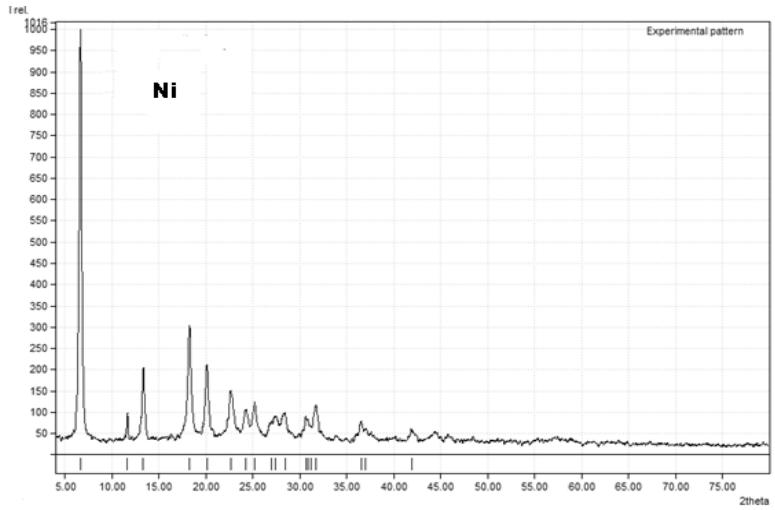


**Fig. 11** (a) XRD pattern of Ni(II) complex (**3**)

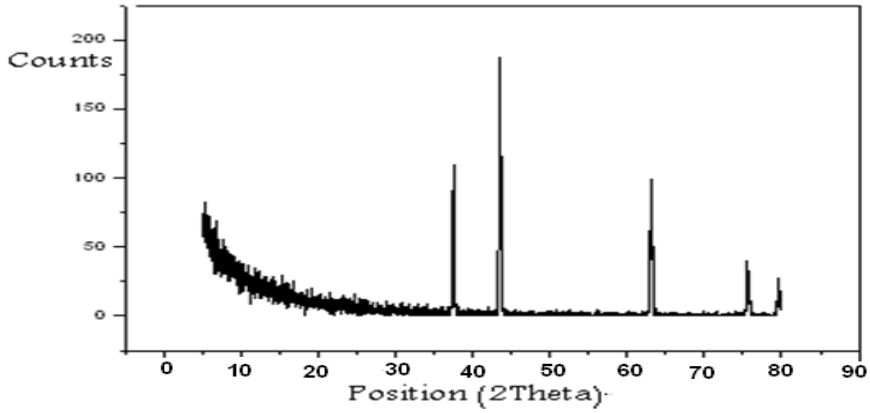


**Fig. 11** *Continued* (b) XRD pattern of solid residue (NiO), resulted from the thermal decomposition of Ni(II) complex (**3**)

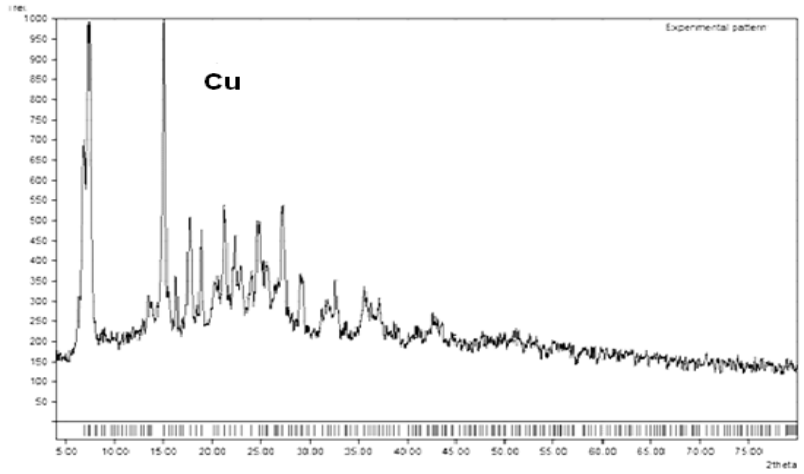


**Fig.12** (a) XRD pattern of copper(II) complex (**4)**

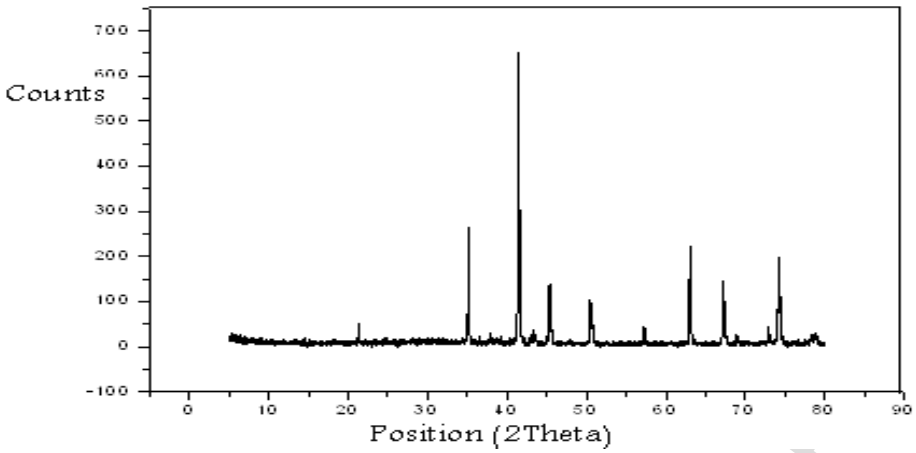


**Fig.12***Continued* (b) XRD pattern of solid residue CuO, resulted from the thermal decomposition of Cu(II)complex (**4**)

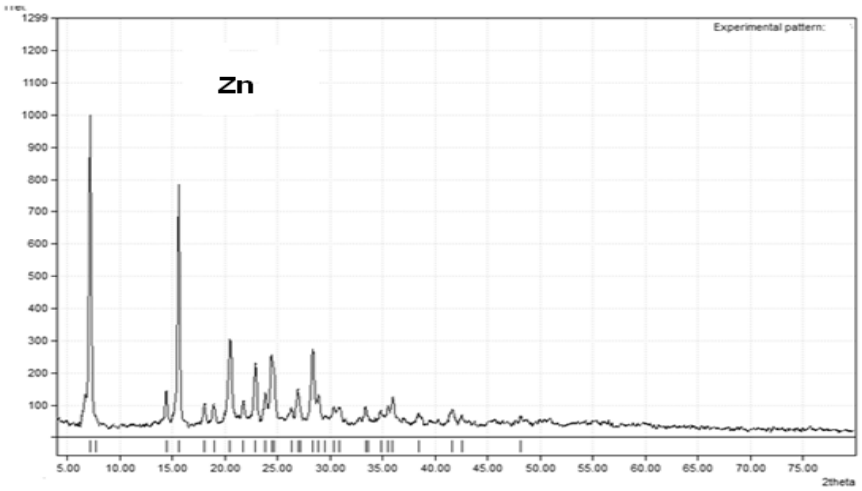


**Fig.13** XRD pattern of Zn(II) complex (5), $[Zn_2(L)Cl_4(H_2O)2].7H_2O$

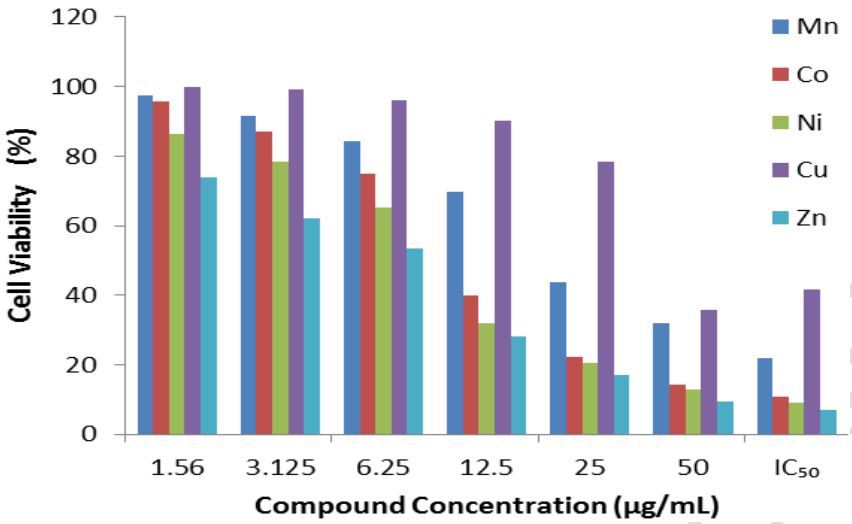


**Fig.14** Biological activity of metal complexes against Hepatocellular Carcinoma cell (Hep-G2)

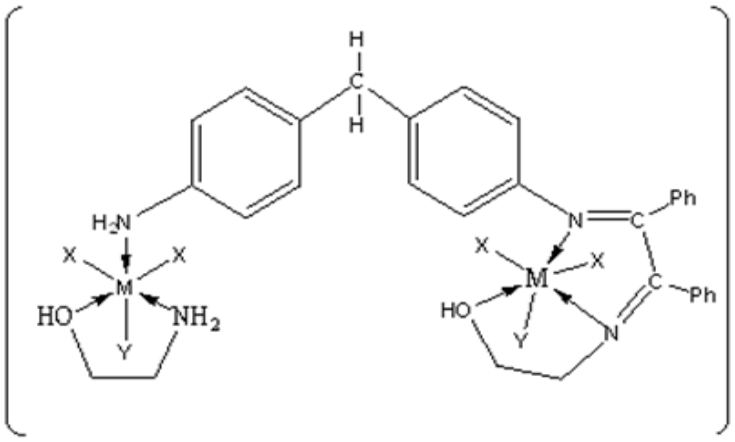


| No | Complex | M | X | Y | n | m |
|---|---|---|---|---|---|---|
| **1** | $[Mn_2(L)Cl_4(H_2O)_2].7.5H_2O.0.5EtOH$ | Mn | Cl | $H_2O$ | 7.5 | 0.5 |
| **2** | $[Co_2(L)Cl_4(H_2O)_2].8.5H_2O$ | Co | Cl | $H_2O$ | 8.5 | – |
| **3** | $[Ni_2(L)Cl_4(H_2O)_2].\ 5H_2O$ | Ni | Cl | $H_2O$ | 5.0 | – |
| **5** | $[Zn_2(L)Cl_4(H_2O)_2].7H_2O$ | Zn | Cl | $H_2O$ | 7.0 | – |

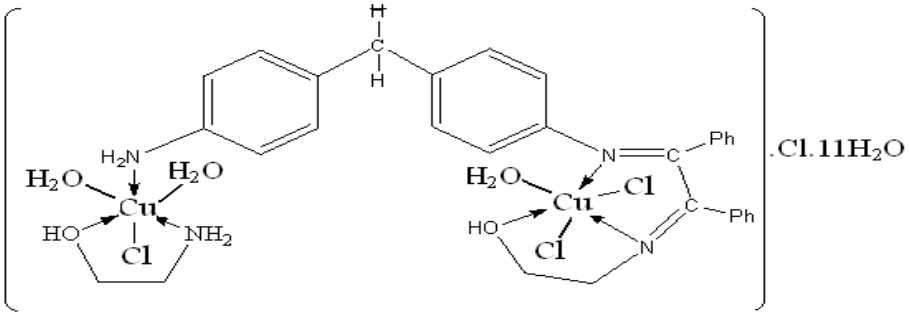


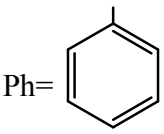


**Scheme 1** Proposed structure for metal complexes

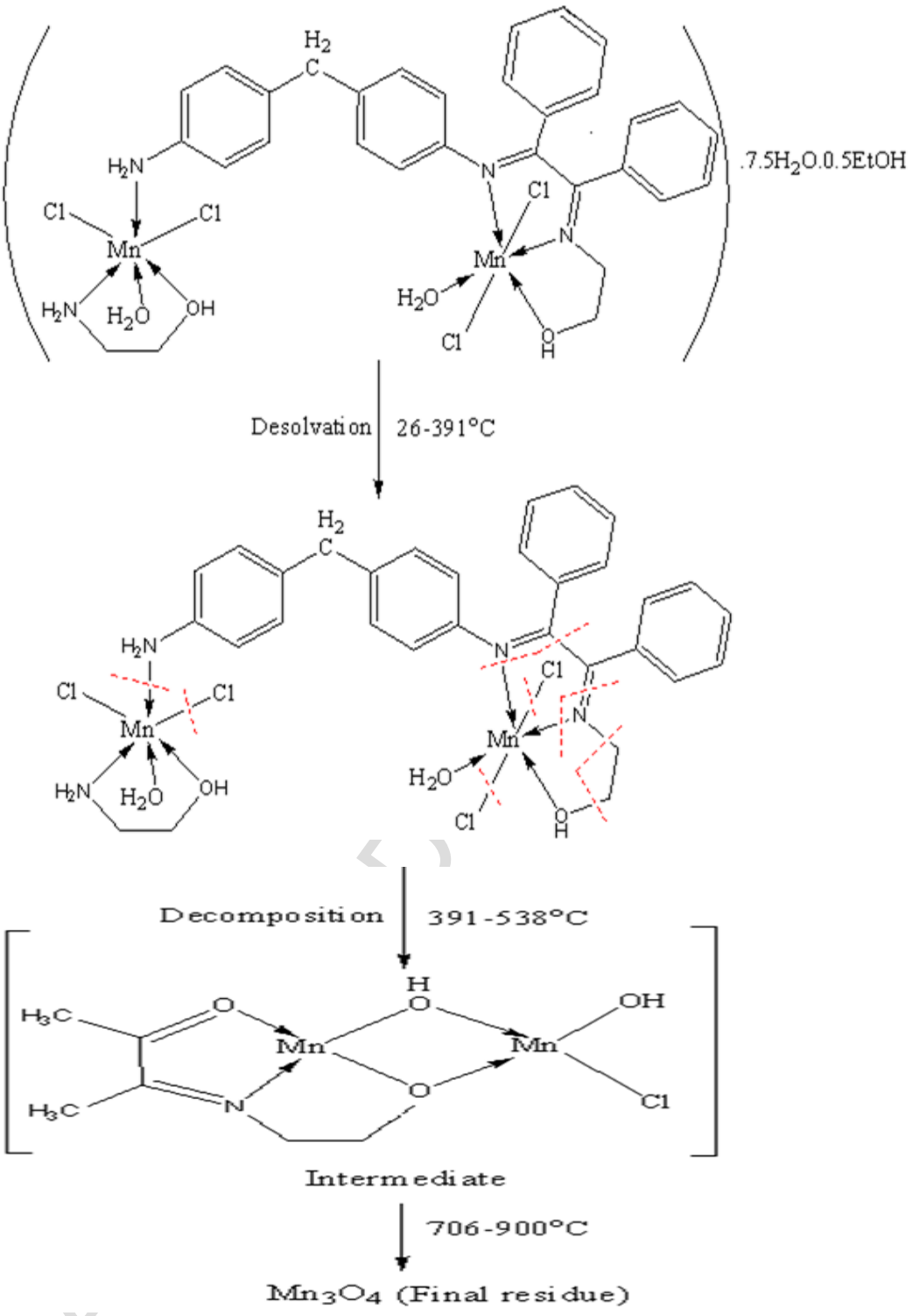


**Scheme 2** Thermal decomposition of complex (**1**) $[Mn_2(L)Cl_4(H_2O)_2].7.5H_2O.0.5EtOH$

**Table 1**
The analytical and physical data of Mn(II), Co(II), Ni(II), Cu(II), and Zn(II) complexes

| No | Compound | F.W. | Elemental analyses Found/(Calcd.)% | | | | | $\Lambda^*$ | Melting point ($^oC$) |
|---|---|---|---|---|---|---|---|---|---|
| | | Color | C | H | N | Cl | M | | |
| **1** | $[Mn_2(L)Cl_4(H_2O)_2].7.5H_2O.0.5EtOH$ | 940.69 | 40.86 | 6.00 | 5.96 | 15.09 | 12.08 | 19 | 349 |
| | $C_{32}H_{56}N_4O_{12}Mn_2Cl_4$ | Brown | (40.98) | (5.77) | (6.17) | (15.63) | (12.09) | | |
| **2** | $[Co_2(L)Cl_4(H_2O)_2].8.5H_2O$ | 934.60 | 39.61 | 5.34 | 6.45 | 15.50 | 12.71 | 11 | 318 |
| | $C_{31}H_{55}N_4O_{12.5}Co_2Cl_4$ | Green | (39.84) | (5.80) | (6.00) | (15.19) | (12.61) | | |
| **3** | $[Ni_2(L)Cl_4(H_2O)_2].5H_2O$ | 880.15 | 42.20 | 5.45 | 6.76 | 16.51 | 13.58 | 14 | 325 |
| | $C_{31}H_{48}N_4O_9Ni_2Cl_4$ | Light brown | (42.31) | (5.50) | (6.37) | (16.13) | (13.34) | | |
| **4** | $[Cu_2(L)Cl_3(H_2O)_3].Cl.11H_2O$ | 1015.87 | 36.97 | 5.83 | 6.03 | 14.50 | 12.61 | 54 | 245 |
| | $C_{31}H_{62}N_4O_{16}Cu_2Cl_4$ | Green | (36.65) | (6.15) | (5.52) | (13.98) | (12.50) | | |
| **5** | $[Zn_2(L)Cl_4(H_2O)_2].7H_2O$ | 929.55 | 39.74 | 5.22 | 6.31 | 16.61 | 13.59 | 8 | 300 |
| | $C_{31}H_{52}N_4O_{11}Zn_2Cl_4$ | Yellowish white | (40.06) | (5.64) | (6.03) | (15.28) | (14.07) | | |

*: $\Omega^{-1}cm^2mol^{-1}$

**Table 2**

Infrared spectral bands ($cm^{-1}$) of Mn(II), Co(II), Ni(II), Cu(II), and Zn(II) complexes

| No. | Complex | $\delta(NH_2)$ | $\nu$(C=C)+ $\nu$(C=N) | $\nu(-CH_2-OH)$ | $\nu(-C-NH_2)$+ $\nu$(M-OH) | Overtone of $NH_2$ + $\nu$(M-N) of $NH_2$ | $\delta$(OH) | $\nu$(M-N) of azomethine |
|---|---|---|---|---|---|---|---|---|
| **1** | $[Mn_2(L)Cl_4(H_2O)_2].7.5H_2O.0.5EtOH$ | 1619 (m,sp.) | 1583 (s,sp.) | 1092 (s,br.) | 1123 (s,br.) | 517 (m) | 1301 (w) | 489 (w) |
| **2** | $[Co_2(L)Cl_4(H_2O)_2].8.5H_2O$ | 1627 (sh.) | 1589 (s) | 1067 (s,br.) | 1105 (s,br.) | 525 (w) | 1309 (w) | 466 (w) |
| **3** | $[Ni_2(L)Cl_4(H_2O)_2].5H_2O$ | 1619 (m,sp.) | 1584 (m,sp.) | 1074 (vw.) | 1103 (s,br.) | 528 (w) | 1321 (w) | 499 (w) |
| **4** | $[Cu_2(L)Cl_3(H_2O)_3].Cl.11H_2O$ | 1611 (m) | 1569 (m) | 1096 (sh.) | 1120 (s) | 538 (w) | 1328 (w) | 489 (w) |
| **5** | $[Zn_2(L)Cl_4(H_2O)_2].7H_2O$ | 1625 (sh.) | 1592 (s) | 1070 (s) | 1128 (s,br.) | 524 (w) | 1324 (w) | 482 (w) |

vw: very weak, w: weak, m: medium, s: strong, b: broad, sh: shoulder, sp: splitted.

**Table 3**
Important bond lengths characterized for Mn(II) complex

| Bond | Bond length(A°) | Bond | Bond length(A°) |
|---|---|---|---|
| Mn(21)–N(18) ethanol | 1.846 | Mn(28)–N(15)MDA | 1.846 |
| Mn(21)–N(14)MDA | 1.846 | Mn(28)–N(29)ethanol | 1.846 |
| Mn(21)–O(24)ethanol | 1.810 | Mn(28)–O(30)ethanol | 1.810 |
| Mn(21)–Cl(25) | 2.160 | Mn(28)–Cl(33) | 2.160 |
| Mn(21)–Cl(26) | 2.160 | Mn(28)–Cl(34) | 2.160 |
| Mn(21)–O(27)$H_2O$ | 1.810 | Mn(28)–O(35)H2O | 1.810 |
| C(16)–C(17) | 1.337 | N(15)-C(8)MDA | 1.266 |
| C(4)ring–N(14) | 1.260 | N(29)-C(31)ethanol | 1.438 |
| C(17)–C(42) | 1.337 | C(32)-O(30) ethanol | 1.402 |
| C(16)–C(36) | 1.337 | N(18)ethanol-C(22)ethanol | 1.470 |
| N(18)ethanol=C(17)benzil | 1.260 | | |

**Table 4**

Electronic spectral data and magnetic moments of Mn(II), Co(II), Ni(II), Cu(II), and Zn(II) complexes

| No. | Compound | Electronic spectral bands (nm) | Assignment | $\mu_{eff.}$ (B.M.) (per metal ion) |
|---|---|---|---|---|
| **1** | $[Mn_2(L)Cl_4(H_2O)_2].7.5H_2O.0.5EtOH$ | 662 | $^6A_{1g} \rightarrow {}^4T_{1g}\,(^4G)$ | 1.61 |
| | | 584 | $^6A_{1g} \rightarrow {}^4E_g\,(^4G)$ | |
| | | 524 | $^6A_{1g} \rightarrow {}^4E_g\,(^4D)$ | |
| | | 466 | LMCT | |
| | | 253,296,324 | π-π*, n-π* | |
| **2** | $[Co_2(L)Cl_4(H_2O)_2].8.5H_2O$ | 680 | $^4T_{1g}(F) \rightarrow {}^4A_{2g}(P)$ | 4.06 |
| | | 580 | $^4T_{1g}(F) \rightarrow {}^4T_{2g}(P)$ | |
| | | 468 | LMCT | |
| | | 252,296,322 | π-π*, n-π* | |
| **3** | $[Ni_2(L)Cl_4(H_2O)_2].5H_2O$ | 725 | $^3A_{2g}\,(F) \rightarrow {}^3T_{2g}(F)$ | 3.11 |
| | | 620 | $^3A_{2g}\,(F) \rightarrow {}^3T_{1g}(F)$ | |
| | | 526 | $^3A_{2g}(F) \rightarrow {}^3T_{1g}(P)$ | |
| | | 438 | LMCT | |
| | | 252,296,321 | π-π*, n-π* | |
| **4** | $[Cu_2(L)Cl_3(H_2O)_3].Cl.11H_2O$ | 662 | $^2B_{1g} \rightarrow {}^2B_{2g}$ | 1.59 |
| | | 541 | $^2B_{1g} \rightarrow {}^2E_g$ | |
| | | 466 | LMCT | |
| | | 252,292,319 | π-π*, n-π* | |
| **5** | $[Zn_2(L)Cl_4(H_2O)_2].7H_2O$ | 516,466 | LMCT | Diamagnetic |
| | | 252,296,320 | π-π*, n-π* | |

**Table 5**

Thermal Studies of Mn(II), Co(II), Ni(II), Cu(II), and Zn(II) complexes

| No. | Compound | TG range (°C) | DTG peak (°C) | Mass Loss % | | Assignment | $T_S$ (°C) |
|---|---|---|---|---|---|---|---|
| | | | | Found | Calcd. | | |
| **1** | $[Mn_2(L)Cl_4(H_2O)_2].7.5H_2O.0.5EtOH$ | 26-391 | 43[f], 349[e] | 16.81 | 16.81 | loss of 0.5 mol of EtOH and 7.5 mol of outersphere $H_2O$[a+b] | 391 |
| | | 391-538 | 484[c] | 48.68 | 49.86 | loss of 4.5 C, $C_{20}H_{18}N_2$, $1.5Cl_2$, $NH_3$ and $2.5H_2$[d] | |
| | | 538-706 | – | 34.80 | 33.33 | Stable zone:( no weight loss due to formation $C_{6.5}H_{12}NO_4Mn_2Cl$)[r] | |
| | | 706-900 | 798[c] | 14.43 | 14.21 | loss of 6C, $NH_3$, $0.5Cl_2$ and $4.5H_2$ gases[d] | |
| | | At 900 | | 20.09 | 19.12 | $Mn_3O_4$ +0.5C[f] | |
| **2** | $[Co_2(L)Cl_4(H_2O)_2].8.5H_2O$ | 27-361 | 51[f] 345[g] | 9.66 | 9.55 | loss of 5 mol of outersphere $H_2O$[a] | 361 |
| | | 361-582 | 449[I] | 59.27 | 59.29 | loss of 3.5 mol of lattice $H_2O$, $C_{25.5}H_{20}N_2$, and $2Cl_2$ gases [d] | |
| | | 582-900 | 747[e] 880[f] | 7.97 | 8.71 | loss of 3C, $6H_2$ and $2NH_3$ gases [d] | |
| | | At 900 | | 23.11 | 22.45 | $Co_3O_4$ + 2. 5C[f] | |
| **3** | $[Ni_2(L)Cl_4(H_2O)_2].5H_2O$ | 31-398 | 52[f] 306[g] | 10.55 | 10.23 | loss of 5 mol of outersphere $H_2O$[a] | 398 |
| | | 398-538 | 464[i] | 32.65 | 32.54 | loss of $C_{20}H_{18}N_2$[d] | |
| | | 538-798 | 678[f] | 38.87 | 38.89 | loss of 2 mol of coordinated $H_2O$, $C_{10}H_{20}N_2O_2$ and $2Cl_2$ gases [d] | |
| | | At 798 | | 19.76 | 18.34 | 2NiO + C[f] | |

[a] :Dehydration, [b] :Desolvation, [d] :Decomposition, [c] :strong, [e] :medium, [f] :weak, [g] :very weak, [h] :broad, [i]:broad strong, f :final residue

**Table 5** *Continued*

| No. | Compound | TG range (°C) | DTG peak(°C) | Mass loss % Found | Mass loss % Calcd. | Assignment | $T_S$ (°C) |
|---|---|---|---|---|---|---|---|
| **4** | $[Cu_2(L)Cl_3(H_2O)_3].Cl.11H_2O$ | 26-251 | 48[f], 73[f] 176[e] | 12.58 | 12.41 | loss of 7 mol of outersphere $H_2O$ [a] | 251 |
| | | 251-378 | 307[c] | 36.56 | 36.56 | loss of $C_{21}H_{22}N_2$, and $Cl_2$ gas [d] | |
| | | 378-445 | – | 10.51 | 10.64 | loss of 4 mol of lattice $H_2O$ and 2 mol of coordinated $H_2O$ [d] | |
| | | 445-543 | 496[c] | 21.89 | 21.87 | loss of one mol of coordinated $H_2O$, $C_8H_9N_2$ and $Cl_2$ gas [d] | |
| | | 543-630 | 587[f] | 6.02 | 6.01 | loss of $1.5H_2$ and 2CO gases [d] | |
| | | At 630 | | 12.50 | 12.51 | 2CuO[f] | |
| **5** | $[Zn_2(L)Cl_4(H_2O)_2].7H_2O$ | 25-333 | 36[f] | 6.69 | 6.78 | loss of 3.5 mol of outersphere $H_2O$[a] | 333 |
| | | 333-394 | 349[c] | 14.61 | 14.42 | loss of 3.5 mol of $H_2O$ and one mol of $Cl_2$[d] | |
| | | 394-600 | 510[l] | 61.60 | 61.29 | loss of 2 mol of coordinated $H_2O$, one mol of $Cl_2$ and $C_{31}H_{34}N_4$ [d] | |
| | | At 600 | | 17.11 | 17.51 | 2ZnO[f] | |

[a] :Dehydration, [b] :Desolvation, [d] :Decomposition, [c] :strong, [e] :medium, [f] :weak, [g] :very weak, [h] :broad, [i]:broad strong, [r] :final residue

**Table 6**

Kinetic parameters of the thermal decomposition of the metal complexes

| No. | Compound | Temperature range (°C) | DTG peak (°C) | n | ΔE*/ KJmol$^{-1}$ | ΔH*/ KJmol$^{-1}$ | A/s$^{-1}$ | -ΔS*/ KJmol$^{-1}$K$^{-1}$ | ΔG*/ KJmol$^{-1}$ |
|---|---|---|---|---|---|---|---|---|---|
| **1** | $[Mn_2(L)Cl_4(H_2O)_2].7.5H_2O.0.5EtOH$ | 26-272 | 43$^{f}$ | 1.39 | 58.02 | 56.43 | 81.68 | 0.2145 | 132.21 |
| | | 272-391 | 349$^{e}$ | 1.34 | 252.88 | 249.46 | 315.17 | 0.2133 | 270.39 |
| | | 391-538 | 484$^{c}$ | 0.79 | 367.57 | 365.78 | 434.02 | 0.2172 | 394.98 |
| | | 537-899 | 798$^{c}$ | 1.28 | 524.78 | 521.87 | 491.47 | 0.2149 | 545.94 |
| **2** | $[Co_2(L)Cl_4(H_2O)_2].8.5H_2O$ | 27-361 | 51$^{f}$ | 1.07 | 44.54 | 41.32 | 79.08 | 0.2134 | 94.52 |
| | | | 345$^{g}$ | 1.21 | 94.81 | 92.43 | 134.55 | 0.2188 | 127.44 |
| | | 361-582 | 449$^{I}$ | 1.15 | 264.24 | 261.91 | 312.27 | 0.2122 | 284.37 |
| | | 582-900 | 747$^{e}$ | 1.31 | 444.13 | 441.92 | 352.87 | 0.2164 | 473.54 |
| | | | 880$^{f}$ | 0.87 | 521.25 | 518.88 | 459.36 | 0.2109 | 567.11 |
| **3** | $[Ni_2(L)Cl_4(H_2O)_2].5H_2O$ | 31-398 | 52$^{f}$ | 1.26 | 92.57 | 80.92 | 158.43 | 0.2119 | 145.13 |
| | | | 306$^{g}$ | 0.91 | 225.23 | 222.10 | 304.91 | 0.2095 | 302.13 |
| | | 398-525 | 463$^{c}$ | 1.37 | 395.12 | 390.93 | 328.29 | 0.2127 | 498.11 |
| | | 525-725 | 678$^{h}$ | 1.63 | 494.46 | 492.46 | 261.70 | 0.2274 | 524.84 |
| **4** | $[Cu_2(L)Cl_3(H_2O)_3].Cl.11H_2O$ | 26-251 | 48$^{f}$ | 0.99 | 26.81 | 24.52 | 51.36 | 0.2206 | 85.19 |
| | | | 73$^{f}$ | 1.58 | 123.71 | 120.97 | 206.71 | 0.2109 | 190.34 |
| | | | 176$^{e}$ | 1.07 | 268.54 | 266.10 | 407.86 | 0.2065 | 327.64 |
| | | 251-378 | 314$^{c}$ | 1.53 | 146.23 | 142.93 | 241.21 | 0.2287 | 163.73 |
| | | 378-543 | 496$^{c}$ | 1.61 | 317.46 | 314.59 | 251.42 | 0.2151 | 349.74 |
| | | 543-630 | 587$^{f}$ | 0.98 | 573.31 | 570.16 | 521.49 | 0.2097 | 649.64 |
| **5** | $[Zn_2(L)Cl_4(H_2O)_2].7H_2O$ | 25-333 | 36$^{f}$ | 1.83 | 120.80 | 118.39 | 250.84 | 0.2078 | 178.64 |
| | | 333-394 | 349$^{c}$ | 1.94 | 224.44 | 220.94 | 212.88 | 0.2150 | 311.45 |
| | | 394-600 | 510$^{I}$ | 1.03 | 457.70 | 455.33 | 410.74 | 0.2104 | 515.28 |

$^{c}$:strong, $^{e}$:medium, $^{f}$:weak, $^{g}$:very weak, $^{h}$:broad, $^{I}$:broad strong

**Table 7**
Effect of MDA and its Schiff base metal complexes against the two land snail species

| No | Compound | $LC_{50}$ (ppm) | |
|---|---|---|---|
| | | *E.vermiculata* | *M.obstructa* |
| | MDA | 62.73 | 49.58 |
| **1** | $[Mn_2(L)Cl_4(H_2O)_2].7.5H_2O.0.5EtOH$ | 311.15 | 296.02 |
| **2** | $[Co_2(L)Cl_4(H_2O)_2].8.5H_2O$ | 331.82 | 303.42 |
| **3** | $[Ni_2(L)Cl_4(H_2O)_2].5H_2O$ | 321.09 | 307.29 |
| **4** | $[Cu_2(L)Cl_3(H_2O)_3].Cl.11H_2O$ | 251.66 | 229.78 |
| **5** | $[Zn_2(L)Cl_4(H_2O)_2].7H_2O$ | 362.85 | 387.04 |

**Table 8**

In vitro anticancer screening of metal complexes against human hepatic cancer cell line Hep-G2

| Compound Concentration (µg/mL) | 1.56 | 3.125 | 6.25 | 12.5 | 25.0 | 50.0 | $IC_{50}$ *(µg/well)* |
|---|---|---|---|---|---|---|---|
| Complex | Cell Viability (%) | | | | | | |
| $[Mn_2(L)Cl_4(H_2O)_2].7.5H_2O.0.5EtOH$ | 97.47 | 91.62 | 84.19 | 69.57 | 43.68 | 31.95 | 21.9 |
| $[Co_2(L)Cl_4(H_2O)_2].8.5H_2O$ | 95.62 | 87.14 | 74.92 | 39.87 | 22.43 | 14.36 | 10.7 |
| $[Ni_2(L)Cl_4(H_2O)_2]. 5H_2O$ | 86.48 | 78.56 | 65.28 | 31.94 | 20.67 | 12.75 | 9.11 |
| $[Cu_2(L)Cl_3(H_2O)_3].Cl.11H_2O$ | 100.0 | 99.02 | 96.18 | 90.27 | 78.44 | 35.86 | 41.7 |
| $[Zn_2(L)Cl_4(H_2O)_2]. 7H_2O$ | 73.96 | 62.12 | 53.41 | 28.18 | 17.06 | 9.43 | 7.09 |